Gold Standard for the Global Goals

Climate Security & Sustainable Development

METHODOLOGY
GS4GG PAA M400-11

SDG 13

CONTRAIL PREVENTION TO REDUCE AVIATION'S NON-CO_2 CLIMATE IMPACTS

Publication Date: 08/07/2026
Version: 1.0
Next Planned Update: 08/07/2029

SUMMARY

This methodology enables technology-based mitigation of atmospheric warming caused by aircraft contrail cirrus, which are clouds composed of ice crystal hydrometeors that act as short-lived climate forcers (SLCFs). When aircraft pass through cold and humid regions of the atmosphere (ice supersaturated regions or ISSR), water vapour in the aircraft emissions triggers nucleation of ice hydrometeors that can persist for many hours, which collectively cause an annual net warming effect across all commercial flights equivalent to approximately 1% of total anthropogenic climate impact (using GWP100 climate metric this equates to ~650 $MTCO_2e$ annually) The methodology provides a process to mitigate contrail cloud radiative forcing by enabling modification of an existing flight plan to avoid ISSR, which lead to persistent warming contrails. The estimated net radiative impact mitigated is converted into CO_{2e}, which is certified as a mitigation outcome.

ACKNOWLEDGEMENTS

This methodology documents the approach developed by Aerospace Carbon Solutions, a GE Aerospace business, coupling the Weather Research & Forecasting (WRF) model with *pycontrails*, an open-source version of the German Aerospace Centre's Contrail Cirrus Prediction Model (CoCiP). In projects funded by the European Space Agency and other bodies, SATAVIA (now part of GE Aerospace's Aerospace Carbon Solutions) has worked with 14 aircraft operators, NASA, and a large original equipment manufacturer to develop the technology, implement in operations, and progress understanding of

contrail formation and climate impact while building on decades of well-validated, peer-reviewed scientific research.

TABLE OF CONTENTS

1| KEY INFORMATION

The following table describes the key information for the application of methodology.

Table 1. Key information

Activity[1] summary	Methodology enables technology-based mitigation of atmospheric warming caused by aircraft contrail cirrus, which are clouds composed of ice crystal hydrometeors that act as short-lived climate forcers (SLCFs).
Type of GHG mitigation measure(s)	☐ Fuel/feedstock switch ☐ Technology switch ☐ GHG destruction ☒ GHG formation avoidance ☐ Engineered carbon dioxide removal ☐ Nature based carbon dioxide removal
Mitigation type	☒ Emission reduction ☐ Emission removals
Applicable activity scale	☒ Micro scale (e.g., ≤10,000 tCO2e per year) ☒ Small scale (e.g., ≤60,000 tCO2e per year) ☒ Large scale (e.g., >60,000 tCO2e per year)
Are the mitigation outcomes under this methodology at risk of reversal?	☐ Yes ☒ No
Sectoral Scope	Transport
Activity Requirement	Not applicable
Activity start date	The earliest date on which the project developer has committed to expenditures related to the implementation of the mitigation activity.
Crediting Period start date	The start date of the Crediting Period is the date of the start of operations or a maximum of two years prior to the date of Project Design Certification, whichever occurs later.
Geographical applicability	Global.
Limitations	NA

[1] The terms 'Mitigation Activity', 'Activity', 'Project' and 'Project Activity' refer to the activity certified by GS4GG and are used interchangeably

2| DEFINITIONS

2.1.1 | The definitions outlined in the GS4GG Glossary and the Activity Requirement shall apply, in addition to those outlined below:

Table 2. Terms and definitions

TERM	DEFINITION
Certified mitigation outcome	Outcomes certified by Gold Standard to recognise climate mitigation achieve by contrail mitigation (flight plan optimisation) activity. Mitigation certified is non-fungible with CO_2 emissions. Outcomes may be assigned to funders in line with GS4GG Requirements and may be applied against sustainability targets where appropriate.
Contrail	Contrails, or condensation trails, are thin, linear, high-level ice crystal clouds which form in the atmosphere behind aircraft through the mixing of engine exhaust water emissions with cold ambient air, leading to localised supersaturation and hydrometeor nucleation.
Contrail Management Technology	A software platform enabling the pre-flight optimisation of Operational Flight Plans (OFP) for the navigational avoidance of Ice Supersaturated Regions (ISSR) where persistent warming contrail formation is likely. Functionality includes the comparison of baseline and optimised OFP for the calculation of achieved climate mitigation for conversion into certified mitigation outcome.
CO_2 Equivalent (CO_2e)	For the Global Warming Potential (GWP) metric, CO_2e is the amount of CO_2 which, if released, would yield the same radiative impact as a contrail within a given time horizon.
End User	Aircraft operators with responsibility for computing, filing, and implementing aircraft OFP.
Ice Supersaturated Regions (ISSR)	Regions of the atmosphere in which relative humidity with respect to ice exceeds 100%, providing favourable conditions for the formation of cirrus clouds and persistent aircraft contrails.
Longwave Radiation (LW)	Radiation in the infrared part of the electromagnetic spectrum, commonly stemming from the absorption and re-emission of radiation by the land, oceans, clouds, and other atmospheric species.
Numerical weather prediction (NWP) modelling	A meteorological approach utilizing high performance computing and mathematical equations to forecast atmospheric conditions such as temperature, pressure, and wind for future timescales.
Operational Flight Plan (OFP)	Documented plan for a flight which would take place in the absence of project activity, detailing flight metadata including aircraft properties, airports, location, flight level, speed, fuel calculations, and relevant meteorological information.
Operational Flight Plan – Optimised (OFP-O)	Documented plan for a flight as optimised using contrail management technology, detailing flight metadata including aircraft properties, airports, location, flight level, speed, fuel calculations, and relevant meteorological information.
Radiative Forcing (RF)	Incoming or outgoing radiative energy quantified relative to a horizontal surface (Wm^{-2}) and the associated net change caused by a given process.

Relative Humidity with respect to Ice (RH_{ice})	The ratio of the actual water vapour content in the atmosphere to the maximum water vapour content that the air can hold at a given temperature, determining the likelihood of ice crystal, contrail, and cirrus cloud formation.
Segment	Portion of a flight path existing between consecutive waypoints.
Short-lived climate forcers (SLCFs)	A set of chemically reactive compounds with short (relative to carbon dioxide (CO2)) atmospheric lifetimes (from hours to about two decades) but characterized by different physiochemical properties and environmental effects. Their emission or formation has a significant effect on radiative forcing over a period determined by their respective atmospheric lifetimes. Changes in their emissions can also induce long-term climate effects
Shortwave Radiation (SW)	Radiation in the near-infrared, visible, and near-ultraviolet parts of the electromagnetic spectrum, originating from the Sun or from the reflection of sunlight by the land, oceans, clouds, and other atmospheric species.
Top-of-Atmosphere (TOA)	The conceptual boundary between Earth's atmosphere and space at around 100km height above surface, where the energy budget of Earth's atmosphere is considered to end.
Water Saturation	Relative humidity above 100% in which the water vapour pressure exceeds the water vapour saturation pressure at a given temperature.
Waypoint	A single, specific pre-defined geographical location (latitude, longitude) used as part of a flight path for an aircraft.
Weather Research & Forecasting Model (WRF)	A state-of-the-art mesoscale numerical weather prediction system developed by the National Center for Atmospheric Research in the USA, applied in both atmospheric research and operational forecasting applications[2].

3| SCOPE, APPLICABILITY AND ENTRY INTO FORCE

3.1 | Scope

3.1.1 | This methodology applies to activities that enable modification of an existing flight plan to avoid ISSR, which lead to persistent warming contrails, mitigating the contrail cloud radiative forcing. The estimated net radiative impact mitigated is converted into CO_{2e}, which is then certified as mitigation outcome.

3.2 | Applicability

The methodology is applicable under the following conditions:

3.2.1 | Contrail ice crystal hydrometeors formed as the result of ice nucleation that act as a SLCF following the passage of an aircraft through ice-supersaturated regions in the atmosphere.

3.2.2 | Sufficient modelling of atmospheric conditions ex-ante and ex-post, as well as the availability and applicability of flight path recordings to ensure high

[2] E.g. *SATAVIA's configuration of WRF includes a cloud microphysics scheme which incorporates explicit prediction of microphysical processes related to clouds and hydrometeors.*

confidence of avoided contrail formation in flown (rather than merely planned) flight trajectories.

3.3 | Safeguards

3.3.1 | The activity shall adhere to The Gold Standard Principles & Requirements and the Safeguarding Principles & Requirements.

3.3.2 | The project shall not undermine or conflict with any national, sub-national or local regulations or guidance relevant to project activity.

3.3.3 | The mitigation created by contrail management activity may be applied where appropriate against sustainability targets and assigned to funders according to GS4GG Requirements.

3.3.4 | Mitigation outcomes are not fungible with other types of Scope 1 and/or Scope 3 liabilities, including CO_2 emissions.

3.3.5 | Mitigation outcomes are certified according to vintage, derived from future methodology updates, such that CMO of differing vintages (i.e. generated with different atmospheric and/or contrail models) will not be directly comparable.

3.3.6 | Mitigation outcomes shall only be assigned upon the condition that participating aircraft operators expand reported inventory to include the non-CO_2 climate impact arising from aircraft contrails (and NO_X and soot) in the form of an annual inventory.

3.3.7 | Projects shall adopt a value-chain approach to retain achieved climate benefit within the aviation industry, such that the right of first refusal to assign mitigation outcome generated via project activity and held by the project developer/project practitioner shall be offered to stakeholders with Scope 1 and/or Scope 3 liabilities arising from aviation activity, including aircraft operators, original equipment manufacturers (OEM), aircraft lessors, aviation finance organisations, aviation fuel producers, air navigation service providers (ANSP), airports, corporate organisations using aviation for transport of people and goods, and other value chain stakeholders. Mitigation outcomes will initially take place outside CORSIA (Carbon Reduction and Offsetting Scheme for International Aviation), which at present exclusively covers CO_2-related aviation impacts.

3.3.8 | Any relevant subset of these stakeholders may become project participants dependent on involvement with the implementation of contrail management activity, e.g. generation of modified flight plans by ANSP, development of in-flight recommendations via OEM and onboard avionics systems, and implementation of modified flight plans by aircraft operators.

3.3.9 | To avoid double counting or double claiming, the project developer/project practitioner shall clearly communicate to all project participants its ownership rights (including fractional rights in cases where ANSP, OEM, aircraft operators, or others participate in project activity on a pre-agreed basis) and intention of claiming some or all of the emissions equivalent impact avoided via the project activity. This must be communicated by contract or clear written assertions in the transaction paperwork. If the project

developer/project practitioner is not the project technology end user, the end user shall be informed and notified that they cannot claim for emission reductions from the project except by virtue of pre-existing shared ownership agreements.

3.3.10 | It is the project developer's/project practitioner's responsibility to ensure that all data and monitoring requirements are met. Thus, the project developer/project practitioner shall make necessary arrangements such that all needed data are available to the end user. To this end, a formal agreement is needed between project participants and the end user or users.

3.4 | Entry into Force

3.4.1 | The date of entry into force is the publication date of this methodology.

4| NORMATIVE REFERENCES

4.1.1 | The following standards, methodologies, tools, and guidelines are normative references for the application of this methodology. Activity developers shall apply their latest valid version.

4.1.2 | References to CDM tools are valid until equivalent tools are published under Gold Standard (GS4GG) or the Article 6.4 Mechanism (A6.4)/Paris Agreement Crediting Mechanism (PACM) which will become effective thereafter.

4.1.3 | GS4GG Standards and Requirements

a. Principles and Requirements
b. Safeguarding Principles and Requirements
c. Community Services Activity Requirements

4.1.4 | GS4GG Methodologies, Standards, and Tools

a. Methodology Standard: Requirements for Additionality Demonstration (V1.0)
b. Methodology Standard: Requirements for Baseline Setting (GS4GG A6 MS400-04) (V1.0)
c. Tool 01: Emissions from Fossil Fuel Combustion (V1.0)
d. Tool 02: Emissions from Freight Transportation (V1.0)

4.1.5 | Other Sources

a. Rules, Modalities and Procedures for the A6.4 Mechanism (RMP), UNFCCC
b. A6.4-AMT-007: Emissions from electricity generation and consumption | UNFCCC

5| ACTIVITY BOUNDARY

5.1 | Activity scope

5.1.1 | This methodology is applicable to activities that involve technology-based navigational mitigation of radiative forcing arising from aircraft contrails, composed of ice crystal hydrometeors, considered here as a species of short-lived climate forcer (SLCF).

5.1.2 | The project may be implemented by any operator of aircraft for which in-service operational data are available and which are flown utilising aircraft performance-based (i.e., to minimise fuel burn) operational flight plans (OFP), i.e. flight plans created using industry-standard software (or an equivalent solution meeting the same requirements) incorporating optimisations for weather, flight time, fuel burn, air traffic control charges, and other parameters. As such, filed OFP (baseline OFP) may be considered as representing the most optimal routes with regard to standard parameters relevant to the cost of flight operations. Flight planning software is typically developed in line with national and regional regulation and guidance provided by organisations like the US Federal Aviation Agency (e.g. in the form of Advisory Circulars). To generate flight plans optimised for contrail management, project implementors may utilise any available contrail management platform that meets project requirements, operating either as a stand-alone optimiser or as an integrated feature within industry-standard software or a suitable equivalent. All tools or platforms capable of utilising the methodology in its final form (i.e. as published by Gold Standard) will meet the requirements to generate Certified Mitigation Outcome Units; responsibility for translatability of requirements via different platforms will rest with individual Project Developers.

5.2 | Activity Boundary and Analysis Overview

5.2.1 | The project boundary can be summarised in the following Model Workflow, which describes the process for assessing the contrail radiative climate impact (expressed in CO_2e) for a given operational flight plan (OFP) using a coupled numerical weather prediction (NWP) model and contrail climate impact model. After the flight has taken place, the process is repeated, using aircraft tracking data to verify the avoided radiative impact relative to the basic original OFP and taking account of fuel burn penalty and hindcast NWP simulation, where applicable.

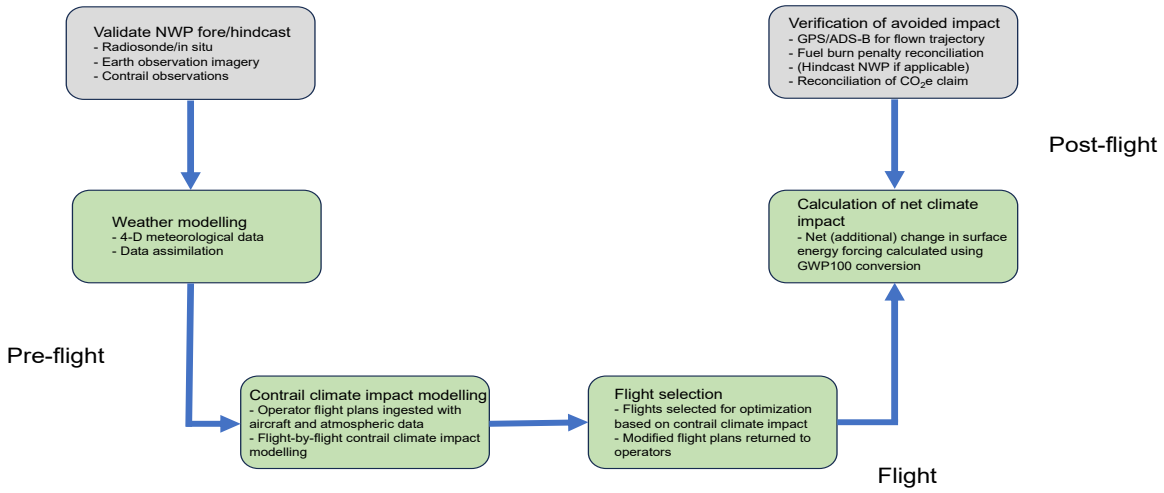

Figure 1 : Analysis Overview

5.2.2 | As shown in Figure 1, above, the NWP model is initialised pre-flight using a global weather data assimilation dataset as input to set initial and boundary conditions and then run over a large geographic region of interest. An initial performance-based OFP planned trajectory is analysed using input parameters (e.g., temperature, pressure, humidity) from the weather forecast generated by a validated NWP model such as WRF. The contrail climate impact model (e.g., CoCiP coded in Python as *pycontrails*) is then run along trajectory location points, and each flight is split into multiple segments, allowing for sector-specific calculations of contrail formation, lifetime, and net radiative impact.

5.2.3 | The underpinning workflow has been developed in trials with multiple aircraft operators, reaching the status of 'flight proven' through multiple successful operations. Further improvements, such as greater automation, are in development and will be incorporated into future model iterations as needed.

5.2.4 | The OFP utilised for the purpose of baselining is taken as the OFP selected for filing by the aircraft operator, rather than as a random selection within the set of possible OFPs generated by (e.g.) industry-standard flight planning software or a suitable equivalent. (In so doing, the methodology follows the approach taken by the European Union Emissions Trading System's Non-CO_2 Aviation Effects Tracking System [EU ETS NEATS] for monitoring, reporting and verification [MRV] of aviation's non-CO_2 climate impacts.) In routine day-to-day operations, tactical deviations rarely exceed 10% divergence from OFP trajectories and normally deviate by 3% or less (e.g. EUROCONTROL horizontal flight efficiency of 97% in 2023), such that baseline OFPs remain the best available source of baseline for comparison with optimised flight trajectories. Recent and future flight plans will continue to provide data to help give confidence in the modelling/counterfactual approach.

5.2.5 | The contrail climate impact modelling approach utilised in the methodology does not require verification in the form of a 'counterfactual' flight flown using

the baseline OFP rather than the modified OFP, a counterfactual which would also be impossible in almost all practical contexts. Instead, the approach requires only the 'counterfactual' of the baseline (non-flown) OFP climate impact generated using a modelling approach.

5.2.6 | To determine the optimal trajectory to minimise the net radiative impact from contrail clouds, locations around the planned flight trajectory are analysed to find the minimal contrail radiative impact (in CO_2e units) while optimising aircraft performance and associated fuel burn and related emissions for a specific aircraft type and engine characteristics. This information is provided back to the operator to enable the generation of a new planned flight trajectory – an optimised OFP - which can be filed with the air navigation service provider (ANSP). This process can also be done tactically in coordination between the ANSP and Air Traffic Control (ATC) and the aircraft operator. The process can be implemented manually or automated through software.

5.2.7 | After the completion of the modified flight, the estimated mitigated radiative impact is verified by conducting analysis on both the original performance-based OFP (baseline) and the actual climate-optimised trajectory from GPS data or transmitted ADS-B (aircraft tracking) data, if GPS data is not available. (Additionally, the NWP model can be rerun to generate hindcast weather data if this approach is demonstrated to add significant value over time (Section 5.2.11 |. c).

5.2.8 | The estimated mitigated radiative impact is then calculated as:

$$mitigated\ impact = CO_2e\ impact\ of\ original\ flight\ plan - CO_2e\ impact\ of\ flown\ flight - change\ in\ CO_2\ emissions\ due\ to\ change\ in\ fuel\ burn$$

5.2.9 | This calculation is expressed as an average over flights taken in a monitoring period in Equation 72 (section 10.1.2 |). The calculations are a function of weather and flight trajectory factors, as summarised in Table 3.

Table 3: summary of inputs for the estimated saving calculation

Input	Variables	Sources	
		CO_2e impact of original flight plan	CO_2e impact of flown flight
Atmospheric environment	Temperature, pressure, humidity, wind vectors	Numerical weather prediction model	Numerical weather prediction model

Aircraft flight trajectory	Time, latitude, longitude, flight level	Baseline OFP	GPS or ADS-B data[3]
Aircraft emissions	Fuel flow (which determines water emissions),	Poll-Schumann model[4], or airline fuel flow data if supplied in the baseline OFP	Poll-Schumann model or post-flight airline fuel flow data if supplied.
	Particulate matter emissions	Particulate emissions models (see appendix)	Particulate emissions models (see appendix)

5.2.10 |The current methodology focuses on reducing aviation's climate impact by reducing the net warming effect caused by aircraft contrail clouds caused by absorption, scattering and emission of outgoing longwave radiation. In future, the approach could also be used for the intentional creation of cooling contrails, i.e., contrails which cause a net cooling effect by reflecting more shortwave (solar) radiation upwards than emission of longwave (thermal) radiation downwards. The methodology is currently not applied to the quantification of cooling effects.

5.2.11 |**Model Requirements**

Any NWP and contrail climate impact models that meet relevant technical requirements can be used. At a minimum, these requirements include the following:

a. NWP models: sufficient model vertical resolution to enable data-based vertical deviations of two flight levels (2,000 feet or approximately 609 metres in the standard atmosphere); appropriate cloud microphysics scheme to allow for accurate predictions of RH_{ice} ≥100%. A strategy to deal with uncertainty in the model prediction is provided in Section 13.5 |.

b. Contrail climate impact models: capacity to account for the factors detailed in the scientific outline below, in order to generate accurate and reliable calculations of contrail climate impact arising from radiative forcing.

c. A hindcast analysis on a horizontal grid spacing of ~ 5km or smaller, to be utilised if this analysis is demonstrated to add >10% accuracy compared to forecast NWP models when validated against atmospheric observations (e.g. radiosonde balloon soundings).

5.2.12 | The spatial extent of the boundary is specified by the atmospheric region through which an individual aircraft passes.

[3] ADS-B stands for Automatic Dependent Surveillance–Broadcast. ADS-B data details an aircraft's location during its flight.
[4] This is an aircraft performance model which is described in section 7.4g below.

5.2.13 |Emissions from aircraft engines shall be modelled, and the difference in flight emissions between original flight plan and revised plan (increased baseline emissions) regarding CO_2 will be included in net climate benefit calculations, excluding non-contrail non-CO_2 effects (e.g. NO_x, aerosol-cloud interactions). The use of pre-tactical weather modelling allows for fine-grained optimisation of flight plans, such that non-CO_2 climate benefits achieved through contrail management flight optimisation at scale outweigh additional CO_2 arising from fuel burn penalties by a significant margin (up to an order or orders of magnitude, as demonstrated in previous flight trials conducted by the Project Developer with a range of partners). In addition, previous trials have utilised minimum thresholds for action (e.g. >10TCO_2e forecast contrail climate impact avoidable via flight optimisation) and maximum fuel burn penalties for optimised routes (e.g. <0.5TCO_2). Taken together, measures such as this ensure that the minimum climate benefit, scaled over multiple flights, will always be large enough to justify contrail management despite small fuel burn penalties.

5.2.14 |Of the six greenhouse gases listed in Annex A of the Kyoto protocol[5] (UNFCCC, 1997a), carbon dioxide (CO_2) and nitrous oxide (N_2O) are emitted by aircraft, carbon dioxide directly and nitrous oxide indirectly via conversion from nitrogen oxides, or NO_x (see Lee *et al*., 2021, for an overview of the non-CO_2 impacts of aviation). Aircraft engines also emit other species relevant to climate forcing. The key quantities include:

a. H_2O vapour emissions which convert to hydrometeors in the engine exhaust plume (included in the project boundary and quantified).

b. CO_2 emissions which accumulate in the atmosphere over decades to centuries and cause a rise in global mean temperatures through radiative heating. (The difference between original (baseline) OFP and optimised OFP fuel burn and conversion to CO_2 is included in the project boundary and quantified).

c. Nitrogen oxide (NOx) emissions, which may lead to cooling through chemical destruction of CH_4 (a potent greenhouse gas) but predominantly leads to heating through generation of additional O_3 in the stratosphere (not included in project boundary and not quantified).

d. Aerosols, including soot and sulphur species, are uncertain sources of climate forcing. Soot aerosols in particular play a role in contrail formation by acting as nucleation sites for water droplets and/or ice crystals (included in project boundary and quantified as to their indirect effect in contrail formation but not quantified in direct climate forcing effect).

5.2.15 |Computational resources required for numerical simulations used in contrail avoidance can lead to emissions associated with electricity production needed to power servers. Annual climate impact arising from high performance

[5] Carbon dioxide, Methane, Nitrous oxide, Hydrofluorocarbons, Perfluorocarbons, Sulphur hexafluoride

computing (HPC) shall be calculated and deducted from claims of net climate impact achieved via contrail management supported by HPC.

6| DEMONSTRATION OF ADDITIONALITY

6.1.1 | The project developer/project practitioner shall demonstrate that the project would not take place without project development finance. Possible reasons for the need for monetisation of avoided climate forcing may be that the initial investment or the on-going marketing, distribution, quality control, manufacturing and maintenance costs are otherwise unaffordable for the target population.

6.1.2 | The project developer/project practitioner shall demonstrate additionality by conforming to Methodology Standard - Requirements for additionality demonstration V1.0 with the steps as mentioned in the paragraphs hereinunder.

a. Step 1: Regulatory surplus analysis: Demonstrate that project would not occur due to existing applicable national or international legal requirement.

b. Step 2: Lock-in risk analysis: Not required to be carried out as this is not a GSVER activity.

c. Step 3: Common Practice Analysis: Demonstrate that activity is not widely adopted or common practice in the relevant sector and/or region (e.g. it has low market penetration). The activity would be categorized as TMC-1 (Innovator/Nascent) as the technology is novel, high-cost, and has minimal market presence. Commercial viability is unproven or only demonstrated in pilot projects within the region.

d. Step 4: Financial viability analysis: Demonstrate that the mitigation activity is not financially viable without revenue coming from CMO.

6.1.3 | Step 5: Barrier analysis: As an alternate approach to step 4, demonstrate that implementation of small scale or microscale activity would be prevented by barriers, and the mitigation outcome revenue makes the determining difference for overcoming the identified barriers.

7| BASELINE SCENARIO

7.1 | Identification of the baseline scenario

7.1.1 | To model the properties of aircraft contrails, the methodology is implementing pycontrails, an open-source Python library (Shapiro et al., 2023). pycontrails is based upon the Contrail Cirrus Prediction (CoCiP) model developed by the German Aerospace Centre (DLR) and laid out in detail in Schumann (2012). The formation and initial transport of the contrails in the aircraft wake is modelled based upon research by Holzäpfel (2003). The subsequent evolution of the contrails over time is described using a numerical integrator where the contrail geometry is treated as a Gaussian plume (Schumann, 2012). The net radiative forcing of the contrails throughout their evolution is calculated using an empirical formulation derived from

radiative transfer calculations (Schumann et al., 2012). All modelling steps are informed by atmospheric data from WRF. WRF and pycontrails are open-source and can be checked for further details. Other models are available and can be utilised in place of WRF and pycontrails if they can be demonstrated to exhibit equivalent or superior fidelity to contrail properties.

7.2 | Calculation of baseline emissions/removals

7.2.1 | Set out here is the implementation of the scientific methods detailed in Schumann (2012), Holzäpfel (2003), Schumann et al. (2012), and others, in pycontrails (Shapiro et al., 2023). Running pycontrails in conjunction with the numerical weather model WRF (Skamarock et al., 2019; WRF Community, 2000) enables to predict the radiative forcing of aviation-derived contrails under the baseline scenario for a given operational flight plan (OFP). This is then subsequently converted into CO2 equivalent emissions.

a. Key variables and model outline

7.2.3 | The formation, evolution, and radiative effects of contrails depend on several parameters of the aircraft and of the ambient atmosphere along the flight path.

Atmosphere and contrail properties:

B = Contrail width (m)

D = Contrail depth (m)

L = Contrail segment length (m)

p = Pressure (Pa)

T = Temperature (K)

I = Ice mass mixing ratio (kg kg^{-1})

ρ = Air density (kg m^{-3})

q = Specific humidity (kg kg^{-1})

q_s = Ice saturation specific humidity (kg kg^{-1})

N = Ice particle number per contrail length (m^{-1})

M = Contrail air mass (kg)

μ = cosine of the solar zenith angle

γ = Ratio of specific heat capacities

R = gas constant (J/kgK)

Aircraft properties:

$\dot{m}_f$ = Fuel burn per second (kg s^{-1})

EI_x = Emission index for species x per fuel burn (g kg^{-1})

V = True airspeed (m s^{-1})

Radiative properties:

OLR = Outgoing Longwave Radiation (W m^{-2})

The net LW radiation that is leaving the atmosphere at the TOA (Top of Atmosphere). Sources include objects cooling via emission of radiation (e.g., the surface of the Earth, clouds)

SDR = Solar Direct Radiation (W m^{-2})

The SW (shortwave) radiation from the Sun that is incoming at the TOA.

RSR = Reflected Shortwave Radiation (W m^{-2})

The SW radiation that is reflected from the Earth's surface, or object in the atmosphere, and is upwardly incident at the TOA.

b. Schmidt-Appleman criterion

7.2.4 | The formation of a contrail can be determined by applying the Schmidt-Appleman thermodynamic criterion. The theorem is built on the assumption that ice clouds (which are contrails) form via the freezing of liquid droplets which condense out of the water vapour released by the jet engine (Kärcher *et al.*, 2015). The temperature requirement for the formation of liquid water is more stringent than that of ice. This can be seen in Figure 2, showing that for a given vapour pressure, a lower temperature is needed for liquid water

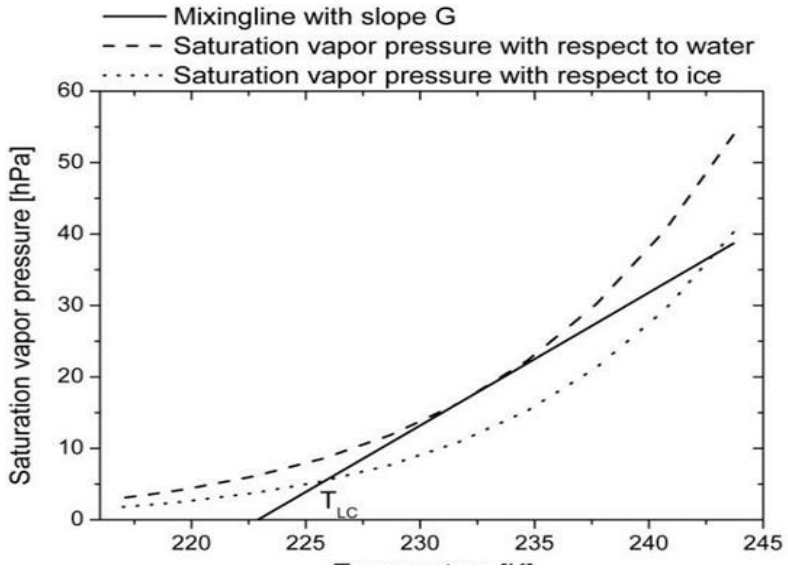

Figure 2: Illustration of the Schmidt-Appleman theory taken from Kaiser et al. (2012)

saturation to be reached than ice saturation. The critical temperature, T_{LC} in

the diagram, is the ambient temperature for which saturation conditions will be reached as the exhaust gases cool down, following the mixing line. If the ambient temperature is greater than this, liquid saturation will not occur in the model and so contrails are unlikely to form.

7.3 | Contrail formation (Stage 0)

7.3.1 | At Stage 0, when contrail formation commences, the initial ice mass mixing ratio, I_0, is taken as the amount of water available in the air above saturation, and is calculated as:

$$I_0 = \frac{4}{\pi}\frac{m_F EI_{H_2O}}{\rho BD} + q - q_s(p,T). \quad (1)$$

Here the first term represents the water produced by the engine, and the second and third terms represent the water vapour in the ambient air above saturation with which the engine exhaust mixes. EI_{H_2O} is the water emission index for burning fuel and is a function of the hydrogen content of the fuel. See Section 13.6.3 | for a model estimating the variation of EI_{H_2O} with the % blend of sustainable aviation fuel (SAF).

7.3.2 | The number of potential nucleation sites is the limiting factor in determining the number of ice particles formed. With aviation fuels derived from kerosene, the number of potential nucleation sites is strongly dependent on the number of soot particles produced (see Schumann, 2012, and references therein). The number of soot particles produced per distance (N_0) is calculated as:

$$N_0 = \frac{\dot{m}_f}{V} EI_{soot} \quad (2)$$

where EI_{soot} is estimated based upon an estimate of the state of the engine, V is the true airspeed of the aircraft[6], and $\dot{m}_f$ is the fuel burn per second. See Section 7.4.48 on the modelling used to estimate EI_{soot}.

7.3.3 | The number of soot particles which are 'activated' and serve as nucleation sites, $N_{0_{act}}$, is modelled to differ from the total number produced to account for the thermodynamic penalties of phase transition:

$$N_{0_{act}} = \left(-0.661 \exp\left(\frac{T - T_{crit}}{T_0}\right) + 1\right) N_0 \quad (3)$$

where $T_0 = 1K$. T_{crit} here refers to the critical temperature from the Schmidt-Appleman criterion (Section 7.2.3). The equation was derived by the *pycontrails* developers from raw data published in Bräuer *et al.* (2021), who discuss in situ measurements of contrail properties (taken during inflight experiments by NASA and DLR) at different altitudes and ambient conditions.

Equation (3) was likely derived from flight test data using a SAF blend of 49% HEFA (hydrotreated esters and fatty acids) with a low sulphur content, by

[6] Therefore a function of the aircraft groundspeed and local windspeed.

mass, of 0.007% (see Figure 3 in Bräuer *et al.* (2021), for plotted flight test data, and Table 1 in Voigt *et al*., 2021, for data on the fuel properties).

In a more recent different flight trial, Märkl *et al*. (2024) reported that burning a 100% SAF blend resulted in reduced activation of ice crystals and suggested the cause of this to be low sulphur fuel content. The fuel had a sulphur content by mass of 0.0007%.

Thus, it is possible that Equation (3), since it is based on a fuel which also has a low sulphur content, though not to the same extent as the 100% SAF fuel, overpredicts the reduction in $N_{0_{act}}$ for regular jet fuel. Further academic work may improve confidence in capturing this impact for a given fuel type and therefore confidence in the constant 0.661 and the prescribed exponential function.

7.4 | Contrail downwash (Stage 1)

7.4.1 | At Stage 1, the ice particles formed during Stage 0 are subsequently transported downwards in the wake of the aircraft. The wake is driven downwards by the aircraft wings due to the generation of lift. Contrails accordingly settle at altitudes tens of metres below the aircraft flight altitude. The physics determining contrail behaviour during downwash operates on such small scales as to be unresolvable computationally in a large model. Additionally, the radiative forcing of contrails predominantly takes place in the time after they have spread out to form high-altitude cirrus clouds (Schumann, 2012). As such, the behaviour of contrails during downwash is prescribed analytically, instead of being modelled explicitly.

7.4.2 | Schumann (2012) derived a parameterisation for the maximum vortex vertical downwash distance, $\boldsymbol{\Delta z_{max}}$, from the Probabilistic Two-Phase Aircraft Wake Vortex Model (Holzäpfel, 2003). Two equations were used depending on the density stratification (which resists the vortex downwash – low density air experiences a buoyancy force when pushed into higher density air). This is captured in the Brunt-Vaisaila frequency, $\boldsymbol{N_{BV}}$[7]:

If $N_{BV} t_0 \geq 0.8$ the strongly stratified equation is used:

$$\frac{\Delta z_{max}}{b_0} = \frac{1.49}{N_{bv} t_0} \tag{4}$$

otherwise, with ϵ^* clipped to be ≤ 0.36,

$$\frac{\Delta z_{max}}{b_0} = 7.68\left(1 - 4.07\epsilon^* + 5.67\epsilon^{*2}\right)(0.79 - N_{BV} t_0) + 1.88 \tag{5}$$

where ϵ^* is the non-dimensional turbulent dissipation rate. It is intuitive that Δz_{max} is a function of this, since the viscous dissipation is the sink of the vortex's kinetic energy. t_0, b_0 and ω_0 are non-dimensional scales of time, wake vortex separation, and initial velocity scale – see Schumann (2012) for their

[7] See pycontrails/pycontrails/physics/thermo on the *pycontrails* (Shapiro *et al.*, 2023) github for its definition.

full definitions. They depend on the aircraft properties of mass and wingspan, as well as the ambient air properties.

7.4.3 | At $N_{bv}t_0 = 0.8$, the strongly stratified equation (5) calculates the non-dimensional quantity $\frac{\Delta z_{max}}{b_0}$ as 1.8625. However, the weakly stratified equation calculates a small range of values depending on the normalized turbulent dissipation rate, ϵ^*, which is limited to be in range (0, 0.36): $1.8032 < \frac{\Delta z_{max}}{b_0} < 1.8593$. Therefore, whilst the two equations do not have perfect continuity, they are close.

7.4.4 | Δz_{max} is used to estimate the initial contrail depth, D_1, which is used to set the initial contrail downwash, Δz_1:

$$\mathrm{D}_1 = C_{D0} \ \Delta z_{max} \tag{6}$$

$$\Delta z_1 = C_{z1}\, \mathrm{D}_1 \tag{7}$$

where C_{D0} and C_{z1} are set to 0.5. *pycontrails* sets the initial width of the contrail, B_1, as

$$B_1 = \frac{\pi}{4} s_a \tag{8}$$

where s_a is the wingspan of the aircraft.

The dependence of the wake vortex model on the wingspan of the aircraft is illustrated in Figure 3, overleaf. A strong correlation is seen between aircraft wingspan and the initial contrail area computed by the wake vortex model. These values were calculated for a given airspeed and atmospheric conditions,

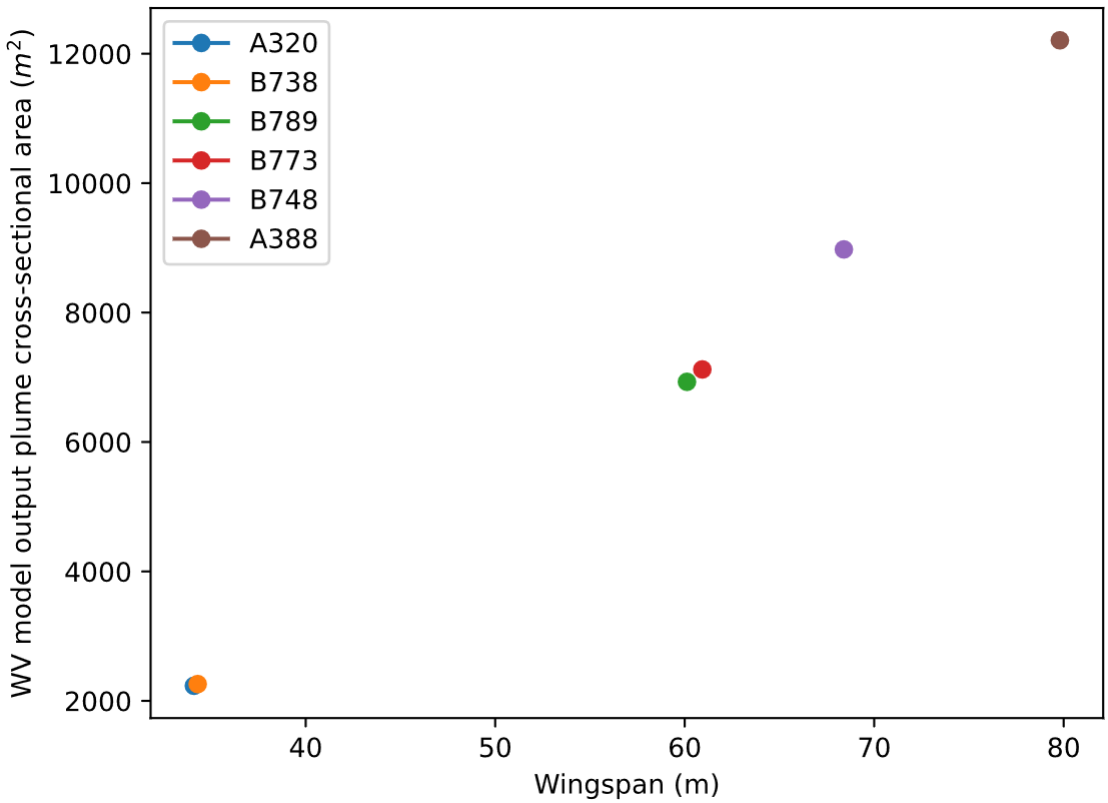

Figure 3 : Variation of contrail cross-sectional plume area perpendicular to the contrail's axis (computed by the wake vortex, WV, model) against aircraft wingspan

but with the mass set to 90% of the maximum take-off mass of the specific aircraft type. Notably, fixing the aircraft mass produced a nearly identical plot, showing the strong dependence of the initial plume area on the wingspan in the model.

7.4.5 | The downwash of the wake vortex leads to an increase in temperature of the contrail through adiabatic warming (Schumann, 2012, and references therein), since the pressure increases. This results in sublimation of a fraction of the ice.

In line with Schumann (2012), *pycontrails* applies an isentropic formula to model the temperature after the wake vortex phase to be

$$T_1 = T_0 \left(\frac{p_1}{p_0}\right)^{\frac{\gamma-1}{\gamma}}. \tag{9}$$

The change in ice content can be estimated using the ice saturation pressure and applying the ideal gas law:

$$\Delta I = \frac{R_d}{R_v}\left(\frac{p_{ice}(T_0+\Delta T)}{p_1} - \frac{p_{ice}(T_0)}{p_0}\right) \tag{10}$$

where R_d and R_v are the gas constants for air and water vapour.

The adiabatic heating of the vortices leads to local subsaturation (with respect to ice) around the ice crystals causing sublimation (Schumann, 2012). Following Schumann, this is modelled by adjusting the number of ice particles using a survival factor, were

$$N_1 \approx f_{surv} N_{0_{act}}. \tag{11}$$

The fraction of surviving ice crystals, f_{surv}, can be approximated as the modelled mass fraction of ice that is not sublimated.

$$f_{surv} = \frac{I_1}{I_0}. \tag{12}$$

The *pycontrails* developers have incorporated a parameterisation for the ice crystal survival fraction presented in Unterstrasser (2016). This was based on high fidelity simulations (Large Eddy Simulations) – more details can be seen within the paper or the *pycontrails* codebase.[8]

c. Contrail evolution (Stage 2)

7.4.6 | At Stage 2, after the downwash process, contrail geometry is described as a Gaussian plume (following Schumann, 2012), meaning that the ice concentration across the vertical cross-section of the contrail plume is a 2D profile described by

$$\boldsymbol{\sigma} = \begin{bmatrix} \sigma_{yy} & \sigma_{yz} \\ \sigma_{zy} & \sigma_{zz} \end{bmatrix} \tag{13}$$

where σ is the covariance matrix of the concentration field, c, in the plane orthogonal to the axis. The width and depth of the 2D profile are defined as

$$B^2 = 8\sigma_{yy} \tag{14}$$

$$D^2 = 8\sigma_{zz} \tag{15}$$

and the area of the modelled cross-section is calculated as

$$A = 2\pi\sqrt{\det(\boldsymbol{\sigma})} \tag{16}$$

The Gaussian plume then evolved through time using a numerical integrator. The plume is advected in all three dimensions due to the wind speed,

$$\frac{\partial x}{\partial t} = U, \quad \frac{\partial y}{\partial t} = V, \quad \frac{\partial z}{\partial t} = W \tag{17}$$

where U is the east-west wind speed, V is the north-south wind speed, and W the vertical wind speed.

In addition to being advected, the plume spreads out horizontally and vertically. This is modelled by assuming a Gaussian solution to the advection-diffusion equations given by Konopka (1995) and cited by Schumann (2012):

$$\sigma_{yy}(t+\Delta t) = \frac{2}{3}S^2 D_V \Delta t^3 + S^2\sigma_{zz}(t)\Delta t^2 + 2\left(D_H + S\sigma_{yz}(t)\right)\Delta t + \sigma_{yy}(t) \tag{19}$$

$$\sigma_{zz}(t+\Delta t) = 2D_V\Delta t + \sigma_{zz}(t) \tag{20}$$

$$\sigma_{yz}(t+\Delta t) = SD_V\Delta t^2 + S\sigma_{zz}(t)\Delta t + \sigma_{yz}(t) \tag{21}$$

[8] https://github.com/contrailcirrus/pycontrails/blob/main/pycontrails/models/cocip/unterstrasser_wake_vortex.py

where S is the shear, defined as

$$S = \frac{dV_n}{dz} \tag{22}$$

and V_n is the plume normal velocity. D_V and D_H are vertical and horizontal diffusion coefficients defined below (Eq. 25 and Eq. 27). In line with Schumann (2012), the shear diffusivity, D_S, not shown above, is set to 0 – see Schumann (2012) for more details.

Vertical diffusivity

7.4.7 | Vertical diffusivity, D_V, is modelled by considering turbulent fluctuations, sedimentation of plume particles, and radiative heating effects on the contrail. Vertical diffusivity is more than an order of magnitude less than the horizontal diffusivity at small timescales (Schumann, 2012) due to the stratification of the atmosphere which inhibits vertical mixing. The ambient turbulence in the atmosphere at cruise altitudes is highly anisotropic with weak vertical turbulent velocities (Schumann *et al*., 1995).

7.4.8 | *pycontrails* deviates from Schumann (2012) by including radiative heating effects. *pycontrails* cite the equations as coming from private communication from Schumann, supplementing published research (Schumann *et al.*, 2010a, b). Radiation emitted from the ground warms up the lower side of the contrail, reducing its density: if the effect is sufficiently strong, this can overcome the stabilizing effect of the density stratification of the atmosphere and lead to turbulent mixing[9]. The vertical mixing rate, or convective velocity scale, with units ms^{-1}, is defined as

$$\omega = \left(\frac{D_{eff}^2 Q_{eff} g}{T} \right)^{\frac{1}{3}}. \tag{23}$$

7.4.9 | Q_{eff} (with units Ks^{-1}) is directly proportional to the differential heating between the top and bottom surfaces of the contrail, Q (Ks^{-1}), but it also depends on the density stratification of the atmosphere which resists vertical mixing:

$$Q_{eff} = Q \frac{\Delta T_{tb}}{\Delta T_{tb} + \frac{1}{2} \frac{dT}{dz} D_{eff}}. \tag{24}$$

7.4.10 |Here ΔT_{tb} is the difference in temperature between the top and bottom of the contrail. This is dependent on two competing effects:

- Longwave radiation from below heating up the base
- Solar radiation from above heating up the top.

7.4.11 |The density stratification is captured by the derivative $\frac{dT}{dz}$, while radiative heating also changes the temperature of the contrail as a whole, and this

[9] See comments in pycontrails/models/cocip/radiative_heating.py on the *pycontrails* github: https://github.com/contrailcirrus/pycontrails/blob/main/pycontrails/models/cocip/radiative_heating.py (Shapiro *et al*., 2023)

enters the equation for ω in T (and affects properties used to calculate I; for example, the saturation humidity, q_s, below).

7.4.12 | If the induced mixing velocity arising from differential heating is below the threshold value of 0.01 ms^{-1}, the vertical diffusivity is modelled as being a result of vertical turbulent fluctuations (the first term in the max function below, c_V[10]) due to, for instance, vertical wind shear.

$$D_V = \max\left(\frac{c_V}{N_{BV}}, \frac{\omega}{N_{BV}}\right) + f_T V_T D_{eff} \quad (25)$$

7.4.13 | In Schumann (2012), c_V was set to 0.002 and it was found that resulting calculations of D_V were consistent with other calculations from the literature[11], over both short time scales (where values tend to be smaller) and long-time scales.

7.4.14 | Whilst shear, S, is prominent in the equation for the plume's growth in the y axis (Eq. 19), explicitly and in the equation for D_H (Eq. 27) (in a slightly different form), it does not feature in the equation for D_V (Eq. 25) or σ_{zz} (Eq. 20). Dürbeck and Gerz, 1996, modelled the dynamics of aircraft exhaust plumes (contrail physics was not considered) using Large Eddy Simulations, and compared these results to the Gaussian plume model described above to estimate values for the diffusivity coefficients. In their model, shear did not impact the vertical diffusivity significantly other than when fully developed turbulence was simulated, for which D_V increased by a factor of 20 relative to simulations with weaker turbulence.

7.4.15 | The simulation of strong turbulence corresponded to a Richardson Number, Ri, of 0.36. Ri quantifies the ratio of the stabilising effect of stratification to the turbulence inducing effect of shear (Galperin *et al*., 2007), and is defined as

$$Ri = \frac{N_{BV}^2}{S_T^2} \quad (26)$$

7.4.16 | The large increase in D_V at this low Ri was somewhat captured by the simple model of Equation (25), despite not being a function of shear, as the low value of N_{BV} increased $\frac{c_V}{N_{BV}}$ by a factor of 10 relative to the weakly turbulent simulations (at higher Ri values).

7.4.17 | Dürbeck and Gerz (1996), stated that fully developed turbulence at typical aircraft altitudes is very rare. However, an additional consideration in the case of contrail plumes is ambient cirrus. Immler *et al*., 2008, reporting results from a lidar measurement campaign in Germany in 2003, noted that persistent contrails were frequently observed to be inside cirrus clouds (thin or subvisible). The dynamics of cirrus cloud systems are complicated, with

[10] This is slightly different notation to Schumann (2012) as here the coefficient is combined with an estimated turbulent vertical velocity.
[11] The studies include Dürbeck and Gerz, 1996, and Schumann et al., 1995, with the latter giving estimated diffusivities calculated from in-flight measurements of aircraft plumes over the North Atlantic, with data taken between 5-100 minutes after plume formation. By utilising a Gaussian plume model, they obtained values in the range of $D_V = 0 - 0.6 m^2 s^{-1}$.

velocity perturbations resulting from small scale convective cells, gravity waves, quasi-two-dimensional waves, and mesoscale waves (Gultepe and Starr, 1995). Gultepe and Starr (1995), found instances of strong updrafts and Ri numbers as low as ~ 0.1 in the in-flight measurements, similar to the value of 0.13 in the highly turbulent simulation in Dürbeck and Gerz (1996). Citing these and other studies, Schumann and Graf (2013), increased c_V by a factor of 5 to capture the impact of stronger turbulence in cirrus clouds. This value is used in *pycontrails*.

7.4.18 |The second term in Equation (25) accounts for the sedimentation of the ice crystals, which increases the vertical depth of the contrail (Schumann, 2012, and references therein): f_T is the sedimentation impact factor, and V_T is the terminal velocity modelled using a parameterisation from Spichtinger and Gierens (2009). D_{eff} differs from the depth, D, to account for the shearing of the contrail profile – see Figure 1 of Schumann (2012).

Horizontal diffusivity

7.4.19 |Horizontal diffusivity, D_H, is driven by the vertical velocity gradients (shear) acting on the contrail, and is defined as

$$D_H = c_H D^2 S_T \tag{27}$$

where c_H is a constant and S_T is the total shear:

$$S_T^2 = f_s^2 \times \left(\left(\frac{dU}{dz}\right)^2 + \left(\frac{dV}{dz}\right)^2 \right) \tag{28}$$

Shear is important as it both changes the shape of the contrail plume and induces turbulence causing the plume to grow faster (Schumann, 2012). The total shear term drives turbulence generation (ibid). Dürbeck and Gerz, 1996, found shear to be the dominating process in determining the horizontal spread of a plume. They simulated two plumes with very different degrees of turbulence but identical shear and found that the horizontal spread of the plume was almost identical.

f_s above is the shear enhancement factor, included following Schumann (2012) to account for subgrid velocity fluctuations not captured in the NWP model. This is also applied to the plume-normal velocity-based shear below. It is defined as

$$f_s = \frac{1}{2}\left(1 + \left(\frac{\Delta z_{eff}}{D}\right)^n\right) \tag{29}$$

where n is a constant set as 0.5 in *pycontrails*, and Δz_{eff} is the effective resolution for shear, set to 2000m (see Schumann 2012 and references within).

7.4.20 |The effect of horizontal wind shear on horizontal diffusion is not accounted for in this model, which is a reasonable approximation in the upper troposphere, where vertical wind shear largely dominates over horizontal wind shear[12].

7.4.21 |The use of a Gaussian plume model to calculate diffusion of the contrail into the ambient atmosphere implies assumption of isotropic growth of the contrail in the vertical and horizontal, respectively. This approach may be an oversimplification, especially at the beginning of the simulation (i.e. in young contrails), but it yields realistic macro- and microphysical properties of the contrail (Schumann, 2012). The Gaussian plume model is commonly used for similar applications, e.g. simulating the spreading of atmospheric pollutants such as industry exhaust plumes.

Ambient meteorology (temperature, wind), which drives diffusion is provided by NWP models which operate at a much coarser spatial grids and time resolutions than contrail models. This motivates limiting the detail of the contrail model to an extent due to potential errors arising from the weather inputs.

7.4.22 |The air mass, ice mass mixing ratio, and number of ice particles also all change with time due to the plume mixing with ambient air. The mixing of the water mass in the plume with the humidity from the ambient air is of particular importance. The mass of the plume at any given timestep is,

$$M(t) = \rho(t)A(t)L(t) \tag{30}$$

where $L(t)$ is the length of the flight segment. The ice mass mixing ratio will then follow the ordinary differential equation (see Schumann, 2012),

$$\frac{dI}{dt} = \frac{1}{M}\frac{dM}{dt}(q_a - q_s - I) - \frac{dq_s}{dt} \tag{31}$$

where q_a is the specific humidity of the ambient air taken from the NWP model, and q_s is the specific humidity at ice saturation[13] – it is assumed that the contrail is at ice-supersaturated conditions. Even if the ambient air is supersaturated ($q_a - q_s > 0$), which causes the ice crystals to grow, I may still decrease, since it is the mass ratio of ice to air, and the mass of air grows by diffusion. The final term accounts for the change in saturation level: if q_s increases then the air can hold more water vapour, and some ice will subsequently sublimate to bring the plume to ice-saturation.

$I(t + \Delta t)$ is solved numerically: see the *pycontrails* code for the numerical implementation[14]. I is an important variable that enters the radiative forcing

[12] Note: *A calculation of wind shear was performed by SATAVIA on 100 randomly selected points inside a WRF weather simulation over Western Europe. It was found that, on average, shear in the vertical direction was over 100 times greater than shear in the two approximately orthogonal horizontal directions. Shear in each direction was calculated as the magnitude of the gradients of the wind velocities perpendicular to that direction (therefore neglecting shear through a velocity gradient in the specified direction).*

[13] kg of water vapour per kg of dry air

[14] See the function *new_ice_water_content* in pycontrails/models/cocip/contrail_properties.py (Shapiro *et al.*, 2023)

calculations when estimating the effective radius of the ice crystals (Section 7.4.26).

7.4.23 |Lastly, as described by Schumann (2012), the number of ice particles in the plume decreases through turbulent loss (i.e., sublimation of ice due to mixing with ambient air) and through aggregation (i.e., larger ice particles sediment quicker than smaller ones, collide with them, and aggregate),

$$\left(\frac{dN}{dt}\right) = \left(\frac{dN}{dt}\right)_{turb} + \left(\frac{dN}{dt}\right)_{agg} \tag{32}$$

where these terms are defined below:

$$\left(\frac{dN}{dt}\right)_{agg} \propto -\frac{E_A 8\pi r^2 V_T}{A} \tag{33}$$

$$\left(\frac{dN}{dt}\right)_{turb} \propto -E_T\left(\frac{D_H}{\max(B,D)^2} + \frac{D_V}{D_{eff}^2}\right) \tag{34}$$

E_A and E_T are coefficients, and the area A is evaluated from the gaussian plume.

$N(t+\Delta t)$ is calculated analytically as,

$$N(t_+) = \frac{N(t)\beta \exp[-\beta\Delta t]}{\beta + \alpha\, \mathrm{N(t)}(1-\exp[-\beta\Delta t])} \tag{35}$$

Where,

$$\alpha = -\frac{1}{N^2}\left(\frac{\partial N}{\partial t}\right)_{\text{agg}} \quad , \quad \beta = -\frac{1}{N}\left(\frac{\partial N}{\partial t}\right)_{\text{turb}} \tag{36}$$

See the pycontrails code for the exact implementation, which accounts for the scenario of $\exp[-\beta\Delta t]$ being very small.[15]

f. Radiative forcing and conversion to CO_2e

Radiative forcing

7.4.24 |The radiative forcing (RF) of a contrail is the net change in shortwave (SW) and longwave (LW) radiation caused by the contrail's presence,

$$RF = RF_{SW} + RF_{LW.} \tag{37}$$

Performing detailed radiative transfer (RT) calculations for each individual contrail to obtain this RF is not computationally efficient. Hence, a parameterised model developed by Schumann *et al.* (2012) is used instead - a set of 15 model parameters which depend only on the ice crystal geometry were created from thousands of RT calculations, accounting for variation in contrail properties, the ambient atmosphere around contrails, and the surface of the planet, within physical ranges. Individual contrail properties and atmospheric

[15] See function *new_ice_particle_number* in pycontrails/models/cocip/contrail_properties.py (Shapiro *et al.*, 2023)

variables are then fed into the parameterised model to obtain RF values efficiently from these empirical equations. RF is calculated as the net addition of downwards radiation.

7.4.25 |Schumann *et al*. (2012) list the main independent properties which the SW and LW forcing depend on and provide their definitions. For shortwave radiation these are:

$$RF_{SW} = f\left(OLR, T_{contrail}, \tau, r_{eff}, \tau_c\right) \quad (38)$$

where OLR is the outgoing longwave radiation, $T_{contrail}$ is the temperature of the contrail, τ is the contrail optical depth (Section 7.4.28), r_{eff} is the effective radius of the ice crystals (see below), and τ_c is the optical depth of cirrus clouds above the contrail. Both optical depths are defined at a wavelength of 550nm.

For longwave radiation:

$$RF_{LW} = f\left(SDR, \mu, A_{eff}, \tau, r_{eff}, \tau_c\right) \quad (39)$$

where SDR stands for the solar direct irradiance, $\mu = \cos(\theta)$ where θ is the solar zenith angle, and A_{eff} is the effective albedo of the earth-atmosphere system (defined as RSR/SDR).

SDR, OLR, and μ are radiation variables, whilst τ_c depends on above cirrus. In this section, the parameterised models used to capture the relationship between these variables and RF_{SW} and RF_{LW} are shown, and some insight into the physical meaning of the different terms is provided. Firstly, further details are provided about the optical depth, τ, the role of different ice crystal geometries, and the effective radius, r_{eff}, terms.

Radiation variables from NWP models

7.4.26 |There are three key radiation quantities in the calculation of a contrail's radiative forcing, two of which are dependent on meteorology. The quantities are given at the 'top of the atmosphere' (TOA), which in a weather model is defined as the highest model level. In previous WRF simulations it has been defined at 80hPa (approximately 64,000 feet, or 19,507 metres, in the standard atmosphere).

- OLR – Outgoing longwave radiation. This is the flux of longwave radiation exiting the top of the atmosphere. It is dependent on the infrared radiation emitted by the Earth's surface as well as the blocking of that radiation by ambient clouds.
- SDR – Solar direct radiation. This is the flux of solar radiation entering the top of the atmosphere. *pycontrails* is able to calculate this directly with no weather modelling required since it depends on factors like time of day and the Earth's orbital position.[16]

[16] See the solar_direct_radiation function for more details:
https://github.com/contrailcirrus/pycontrails/blob/main/pycontrails/physics/geo.py

- RSR – Reflected solar radiation. Shortwave radiation from the sun is reflected by clouds and the Earth's surface back towards space. RSR is the net reflected radiation exiting the top of the atmosphere.

Contrail optical depth, τ

7.4.27 |A key variable in determining the radiative forcing from a contrail is its optical depth, τ. Schumann (2012), presents this as a function of quantities including the effective radius, r_{eff} (see below), the ice mass mixing ratio, I, the effective depth of the contrail, D_{eff}[17], and the radiation extinction efficiency, Q_{eff}:

$$\tau = \frac{3Q_{ext}\rho I}{4\rho_{ice}r_{eff}}D_{eff}. \quad (40)$$

pycontrails uses a manipulated version of this equation. Q_{eff} is calculated, following Schumann (2012), with approximate Mie-theory as

$$Q_{ext} = 2 - \left(\frac{4}{\rho_\lambda}\right)\left(\sin(\rho_\lambda) - \frac{1-\cos(\rho_\lambda)}{\rho_\lambda}\right) \quad (41)$$

where ρ_λ is the phase delay of the light wave propagating through the ice crystal[18].

Ice crystal habits and effective radius, r_{eff}

7.4.28 |As the contrail develops, and the number and size of ice crystals changes, the mean volume radius, r_{vol}, of the ice crystals changes. r_{vol} is calculated in *pycontrails* as

$$r_{vol} = \left(\frac{3}{4\pi}\frac{I}{\rho_{ice}}\frac{A\rho_{air}}{N}\right)^{\frac{1}{3}} \quad (42)$$

Where A is the area of the plume as defined in Equation (16). The equation for r_{vol} can be derived by considering the total volume of ice in the contrail, and the total number of ice crystals.

The ice crystal structure may also change over time. Schumann *et al.* (2011) estimated how the weighting of ice crystal geometries, between 6 different geometries, varies with r_{vol} – Table 4 in their publication is reproduced below[19].

[17] This is defined as the effective cross-sectional area divided by the width.
[18] See the function *light_wave_phase_delay* in pycontrails/models/cocip/contrail_properties.py (Shapiro *et al.*, 2023)
[19] The constants are also laid out in *pycontrails/models/cocip/cocip_params.py* in the github (Shapiro *et al.*, 2023) – here two other geometries are included (the first and last columns) but their weightings are all set to 0. The additional two geometries correspond to spheres and Myhre, which are covered in the parameter's values given in Table 1 of Schumann *et al.*, 2012.

Table 4: Ice crystal structures weighing for different bands of radius, reproduced from Schumann *et al*. (2011), Table 2.

$r(\mu m)$	Solid hexagonal column	Hollow hexagonal column	Rough aggregate	Spatial bullet rosette with six branches	Hexagonal plate	Droxtal
5	0	0	0	0	0	100
9.5	30	0	0	0	0	70
23	30	0	0	30	0	40
190	50	0	0	15	35	0
310	45	45	10	0	0	0
∞	0	0	3	97	0	0

Modelling the ice crystal geometries is important as they influence radiative forcing. The 15 model parameters embedded in the RF_{SW} and RF_{LW} equations are constructed to be purely a function of ice crystal geometry – see Table 1 in Schumann *et al.* (2012).

Effective radius of the ice crystals, r_{eff}

7.4.29 |The ice crystal geometries also affect the effective radius of the ice crystals. The effective radius of ice particles is the variable through which the particle surface area enters the parameterisation. It is defined, in Schumann *et al.* (2011), as:

$$r_{eff} = \frac{3\bar{V}}{4\bar{A}} \tag{43}$$

where $\bar{V}$ and $\bar{A}$ are the mean volume and projected area of particles in a contrail averaged over the size range and weighted by the number density[20]. The size distribution of ice crystals in the contrails is not modelled in *pycontrails* and so calculating r_{eff} with the equation above is not possible. Therefore, to obtain a value for r_{eff}, a model is used to set a scaling factor between the mean volume radius r_{vol} and r_{eff}, C, since r_{vol} can be calculated from the bulk properties of the contrail (Section 7.4.29). C is defined as

$$C = \frac{r_{vol}}{r_{eff}}. \tag{44}$$

Schumann *et al*. (2011) identified the ice crystal habit (the 3D geometry of an ice crystal) as an important factor to take into account when modelling C. In

[20] As defined in Schumann *et al*., 2011, $\bar{V} = \int V_p(D) n_p(D) dD$ where $V_p(D)$ is the mean particle volume for a given diameter, and $n_p(D)$ is the number of ice particles per unit volume of air in size interval $D \to D + dD$. $\bar{A}$ is identically defined but with $A_p(D)$.

pycontrails, functions developed by Schumann *et al*. (2011)[21] estimating C_{habit}[22] for a single particle of a given ice geometry, are used as an estimate of C. These functions take r_{vol} as an input. Thus, for a given r_{vol}, by using Table 4, and the functions from Schumann *et al*. (2011), the effective radius of the different ice crystal habits modelled to be present in a given contrail segment is estimated.

r_{eff} enters the radiative forcing calculations explicitly in the equations below. The radiative forcing is calculated for each ice crystal geometry separately. Additionally, the contrail optical depth also depends on r_{eff} (see above), although in this case a constant for C of 0.9 is used to convert to r_{vol}.

It is intuitive that the radiative forcing would depend on the ice crystal geometry, since the radiative forcing depends, in part, on how much radiation is scattered by the contrails (Schumann *et al.*, 2012).

Calculating the net RF

7.4.30 |The total radiative forcing is found by weighting the radiative forcing contributions from each habit (Schumann *et al*., 2012):

$$RF = \sum_{habits} G_{habit} RF_{habit} \tag{45}$$

where G_{habit} is the different weightings of the habits, such that they sum to 1:

$$\sum_{habits} G_{habit} = 1\,. \tag{46}$$

7.4.31 |The model for the contrail's effect on LW accounts for three physical effects, following Schumann *et al.* (2012). The description below is built upon their explanation.

$$\mathrm{RF_{LW}} = \left(\mathrm{OLR} - k_T(T - T_0)\right) \times (1 - \exp[-\delta_T \tau F_{\mathrm{LW}}(r_{\mathrm{eff}})]) \times (\exp[-\delta_{lr}\tau_c]) \tag{47}$$

Outgoing longwave radiation (OLR) is the infrared or thermal radiation emitted by the Earth and exiting the atmosphere after absorption by ambient clouds, water vapour, and other atmospheric gases (carbon dioxide, ozone, nitrous oxide, methane, oxygen, nitrogen, and halocarbons).

The upward longwave radiation flux from the Earth's surface depends on both the surface temperature ('skin temperature') and the surface emissivity. The spatiotemporal distribution of these two variables is primarily governed by solar irradiance (i.e. the amount of direct sunlight that reaches and heats the Earth's surface) and by land use (e.g. deserts typically have lower emissivity than vegetation, water, and ice). The upward longwave radiation at the Earth's surface is provided by the numerical weather prediction model, which simulates the surface temperature with high spatiotemporal resolution, but also includes seasonal and regional variations in emissivity based on global monthly

[21] They were created from data summarised by Yang *et al*., 2000. These exist in *pycontrails* in pycontrails/models/cocip/radiative_forcing.py (Shapiro *et al.*, 2023)
[22] The ratio of r_{vol} and r_{eff} for one crystal of a particular ice habit.

climatologies of land use. Moreover, by use of a coupled aerosol-cloud-precipitation-radiation parameterisation, the NWP model accounts for the reduction in OLR at the top of the atmosphere due to absorption by model-predicted clouds, water vapour, and other greenhouse gases. More specifically, the cloud microphysics scheme (Thompson & Eidhammer, 2014) used in the NWP model informs the radiation transfer scheme (Iacono *et al*., 2000) about the cloud physical properties (e.g. ice and liquid content and effective radii of particles), as well as the cloud and aerosol optical properties (i.e. optical depth), to calculate total cloudy radiance.

The first bracketed term models the change in OLR if the contrail were opaque, where T_0 is the atmosphere's black-body temperature, and the linear coefficient k_T is a model parameter. The longwave radiation flux entering the atmosphere is not accounted for as it is low.

The second term accounts for how efficient the contrail is at radiating away the energy that it has absorbed, where

$$F_{\text{LW}}(r_{\text{eff}}) = 1 - \exp[-\delta_{lr}\, r_{\text{eff}}] \tag{48}$$

describes the extinction of longwave radiation via absorption and scattering, which depends on the effective radius of the ice crystals that form the contrail. δ_T and δ_{lr} are constants that depend on the ice crystals habits within the contrail, and τ is the optical depth of the contrail detailed above.

The third term specifically accounts for the reduction in OLR due to the existence of ambient cirrus clouds above the altitude of the contrail, with δ_{lr} being another habit-dependent constant. This term may be necessary if the OLR calculated by the weather model does not include the impact of cirrus clouds on upward longwave radiation. The optical depth of the contrail cirrus cloud, τ_c, is estimated using the ice-water content of the atmosphere supplied by the weather model. All the habit specific constants are taken from Schumann *et al*. (2012).

7.4.32 |The contrail's effect on SW can be broken down into four terms,

$$\text{RF}_{\text{SW}} = -\text{SDR} \times (t_A - A_{\text{eff}})^2 \times \alpha_c(\mu, \tau, r_{\text{eff}}) \times E_{\text{SW}}(\mu, \tau_c) \tag{49}$$

Shortwave direct radiation (SDR) is the downwards solar radiation in the absence of alterations through atmospheric interactions. Atmospheric extinction of shortwave radiation occurs through absorption, reflection, and scattering by atmospheric gases (water vapour, carbon dioxide, ozone, methane, oxygen, nitrogen) and by aerosols. These processes are accounted for in the numerical prediction model via coupling of the cloud microphysics and radiative transfer schemes.

The upward shortwave radiation flux is the reflected solar radiation (RSR) due to the albedo (i.e. reflectivity) of the Earth's surface and of the atmosphere itself (i.e. clouds, aerosols), both of which are included in the NWP model. The Earth's surface albedo is an input to the NWP model in the form of a global monthly climatology, so that seasonal changes in, for example, snow cover, vegetation, or land use are accounted for. Cloud albedo is derived from quantities such as the cloud microphysical properties, which are calculated in the NWP model through the cloud microphysics scheme.

A_{eff} is the effective albedo of the earth-atmosphere system, defined as RSR/SDR: if $A_{eff} = 1$, all the solar radiation entering the atmosphere is reflected back to space – similarly if $A_{eff} = 0$, none of the radiation is reflected. A high A_{eff} reduces the impact of a contrail's shortwave forcing because much of the radiation it reflects may have been reflected by the earth-atmosphere regardless.

$\alpha_c(\mu, \tau, r_{\text{eff}})$ can be interpreted as the contrail albedo, and $E_{\text{SW}}(\mu, \tau_c)$ describes the attenuation of SW due to cirrus above the contrail.

Integration and conversion to CO_2e

I. Definitions

7.4.33 |A climate metric is a combination of climate indicator (e.g. Average Temperature Response (ATR) or Global Warming Potential (GWP)), time horizon (e.g. 20, 50 or 100 years) and emission scenario (e.g. Representative Concentration Pathways, RCP) including background emissions (Fuglestvedt *et al*., 2010). Emission scenarios can be sustained emissions or pulse emissions. In this document we only consider pulse emissions.

7.4.34 |**Definition 1: Absolute Global Warming Potential for a species** x $(\boldsymbol{AGWP_x})$ is defined as the time-integrated radiative forcing $(RF_x(t))$ of that species x over a given time horizon (TH).

$$AGWP_x\,(TH) = \int_0^{TH} RF_x(t)dt \tag{50}$$

7.4.35 |**Definition 2:** Absolute Global Warming Potential for CO_2 $\left(\boldsymbol{AGWP_{CO_2}}\right)$ with time horizon 100 years is defined as:

$$AGWP_{CO_2}(100) = \int_0^{100} RF_{CO_2}(t)dt \tag{51}$$

The unit of $AGWP_{CO_2}(100)$ can be $yr\,Wm^{-2}kg_{CO_2}^{-1}$, which indicates t in the integral is in unit of years. We note that this is the default unit for $AGWP_{CO_2}(100)$, as shown in Table 5. The unit of $AGWP_{CO_2}(100)$ can be also $sec.Wm^{-2}kg_{CO_2}^{-1}$, which indicates t in the integral is in unit of seconds. It can be shown that

$$AGWP_{CO_2}(100)\ sec.Wm^{-2}kg_{CO_2}^{-1} = AGWP_{CO_2}(100)\ yr\,Wm^{-2}kg_{CO_2}^{-1} \times t_{yr}$$

where $t_{yr} = 365 \times 60^2 \times 24\ sec.yr^{-1}$.

7.4.36 |**Definition 3**: **CO_2** is well-mixed in the Earth's atmosphere over long timescales and its **energy forcing** $(\boldsymbol{EF_{CO_2}})$ is defined as follows (Teoh *et al*. 2020):

$$EF_{CO_2}[J] = \int_0^{100} RF_{CO_2}\,dt \times S_{Earth}$$

$$= AGWP_{CO_2}(100) \times t_{yr} \times (TFC \times EI_{CO_2}) \times S_{Earth} \tag{52}$$

Here, S_{Earth} is the surface area of earth (m^2), TFC is total fuel consumption of the flight (kg_{fuel}), and EI_{CO_2} is the CO_2 emission index $(kg_{CO_2}\ kg_{fuel}^{-1})$. Therefore, $(TFC \times EI_{CO_2})$ indicates the total CO_2 emission with unit kg_{CO_2}.

7.4.37 | **Definition 4:** CO_2 energy forcing per unit (kg) mass of CO_2 $(\widehat{EF}_{CO_2})$ is derived from Equation 52,

$$\widehat{EF}_{CO_2}\left[J\ kg_{CO_2}^{-1}\right] = AGWP_{CO_2}(100) \times t_{yr} \times S_{Earth} \tag{53}$$

We chose the "hat" notation to indicate that the EF is for 1 kg of CO_2.

Definition 5: Contrail energy forcing arising from individual flight $(\boldsymbol{EF_{contrail}})$ is defined as the product of the contrail radiative forcing $(RF_{contrail})$, the contrail length (L), and the contrail width (W) integrated over the contrail lifetime (t):

$$EF_{contrail}\ [J] = \int_0^t RF_{contrail} \times L(t) \times W(t)\ dt \tag{54}$$

With

$$RF_{contrail} = RF_{SW} + RF_{LW} \tag{55}$$

where RF_{SW} is the contrail radiative forcing in the shortwave spectrum, and RF_{LW} is the contrail radiative forcing in the longwave spectrum. We note that here $RF_{contrail}$ is a localized radiative forcing for contrail compactly supported on the specific area of the contrail; while the $RF_x(t)$ within the definition of $AGWP$ in Equation 50 & 51 is, in general, the global/regional radiative forcing. $EF_{contrail}$ is almost equal to $AGWP_{contrail}$ (but in a different unit) for time horizons greater than one year (Borella *et al*., 2024).

7.4.38 | In our calculation, $EF_{contrail}$ and $RF_{contrail}$ are both outputs from *pycontrails*. Since Pycontrails does not simulate the rapid tropospheric and stratospheric adjustments triggered by the contrail climate forcing, a **contrail** $\boldsymbol{ERF/RF}$ **factor** is used in our calculation to account for those short-term feedback processes (Borella *et al*., 2024). Here $\boldsymbol{ERF}$ indicates the **effective radiative forcing** which is defined as the radiative forcing after allowing for atmospheric temperatures, water vapor and clouds to adjust, but with surface temperature or a portion of surface conditions unchanged. Thus, ERF includes both the effects of the forcing agent itself and the rapid adjustments to that agent (Hansen *et al*., 2005).

Lee et al. 2021, recommend a global ERF/RF ratio of 0.42 for the computation of contrail effective radiative forcing. This value is an average of ERF/RF ratios from three different research papers, 0.59, 0.31 and 0.35, respectively (Ponater et al., 2005; Rap et al., 2010; Bickel et al., 2020). There are two more recent studies with normalized ERF/RF of 0.42 and 0.55 (Bickel et al., 2025). Including these two results in the average of 5 values results in 0.44. We adopt this global ERF/RF ratio in our calculation.

7.4.39 | Definition 6: Contrail CO_2 equivalent arising from an individual flight $(\boldsymbol{CO_2e})$ is defined as:

$$CO_2e\left[kg_{CO_2}\right] = \frac{(ERF/RF) \times EF_{contrail}[J]}{\widehat{EF}_{CO_2}\left[J\ kg_{CO_2}^{-1}\right]} = \frac{(ERF/RF) \times EF_{contrail}[J]}{(AGWP_{CO_2}(100) \times t_{yr} \times S_{Earth})\left[J\ kg_{CO_2}^{-1}\right]} \quad (56)$$

Table 5: List of constants and variables with units

Variable name	Annotation	Unit
CO_2 energy forcing	EF_{CO_2}	J
CO_2 energy forcing per unit of CO_2 emission	$\widehat{EF}_{CO_2}\ per\ unit\ (kg)\ emission\ of\ CO_2$	$J\ kg_{CO_2}^{-1}$
CO_2 radiative forcing	RF_{CO_2}	$W\ m^{-2}$
CO_2 absolute global warming potential with time horizon 100 years	$AGWP_{CO_2}(100)$	$yr\ W\ m^{-2}\ kg_{CO_2}^{-1}$
Total fuel consumption	TFC	kg_{fuel}
CO_2 emission index	EI_{CO_2}	$kg_{CO_2}\ kg_{fuel}^{-1}$
Number of seconds in a year	t_{yr}	s
Surface area of the Earth	$S_{Earth} = 5.1 \times 10^{14}$	m^2
Contrail energy forcing per flight	$EF_{contrail}$	$J = W\ s$
Contrail radiative forcing per unit area	$RF_{contrail}$	$W\ m^{-2}$
Contrail length	L	m
Contrail width	W	m
Contrail radiative forcing in the shortwave spectrum	RF_{SW}	$W\ m^{-2}$
Contrail radiative forcing in the longwave spectrum	RF_{LW}	$W\ m^{-2}$
CO_2 equivalent in metric ton	$CO_2e\ in\ metric\ ton$	$kg_{CO_2} \times 10^3 = metric\ ton\ CO_2$

II. Choice of climate metric

7.4.40 |There are many different climate metrics and timeframes. Figure 4 overleaf, taken from Borella *et al*. (2024) highlights the different metrics and relative importance of CO_2 versus contrail climate impacts. In terms of timeframe, Borella *et al*. (2024) point out the UNFCCC (United Nations Framework Convention on Climate Change) decided in 1995 for its Kyoto Protocol to

compute CO_2-equivalent emissions of greenhouse gas emissions using a metric definition based on the integration of radiative forcing, called the global warming potential (GWP), over a time horizon of 100 years. That decision was reconfirmed in 2018 (UNFCCC, 1995, 2019).

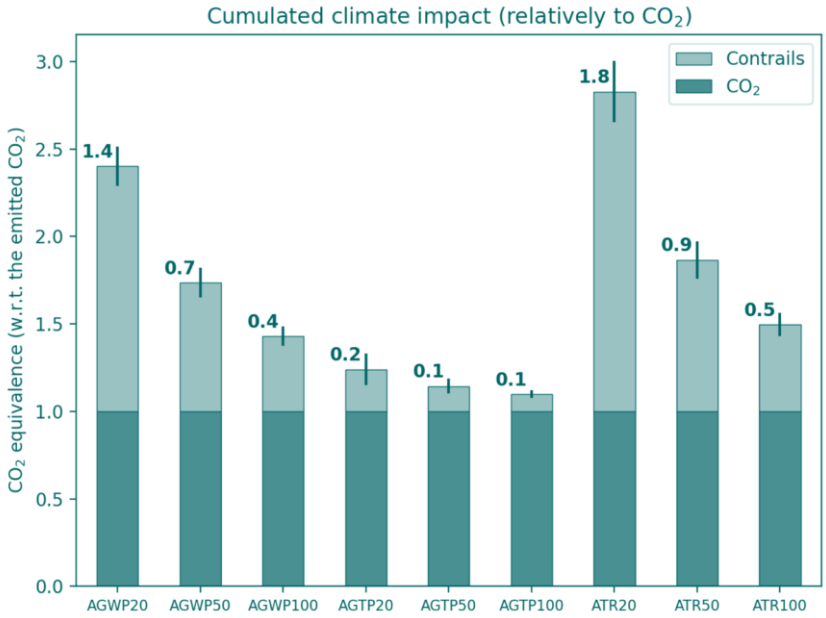

Figure 4 : CO2 equivalence of a median North Atlantic contrail with a contrail efficacy of 0.37 (orange) compared to the emitted CO2 during the median flight (grey) when using absolute global warming potential (AGWP), absolute global temperature change potential (AGTP), and average temperature response (ATR) with time horizons of 20, 50, and 100 years. Error bars quantify the 1σ uncertainty arising from the physical climate and carbon cycle of OSCAR, rather than uncertainties in the contrail radiative forcing and efficacy. The values at the top of each bar are the ratio of non-CO2 to CO2 effects for each metric choice. Taken from Borella et al., 2024.

7.4.41 |In this methodology document we propose that GWP100 is the best choice regarding both timeframe and being the most conservative non-endpoint metric. Of the metrics shown in figure above there are two types – average over timeframe (AGWP and ATR) and endpoint metrics (AGTP). Given that aircraft are going to continuously operate and frequently produce contrails, the endpoint method seems excessively conservative – i.e. to have a pulse emission and then look at impact 100 years later. Of the remaining average over horizon methods, the GWP100 is the most conservative method (smallest contrail vs. CO_2 impact) and therefore appears to be the most appropriate for this methodology.

III. Model and assumptions for $\mathbf{AGWP_{CO_2}(100)}$

7.4.42 |The $AGWP_{CO_2}(100)$ value can be cited from Kyoto Protocol (UNFCCC, 1997), also cited in Joos *et al.* (2013) based on a linear model as

$$AGWP_{CO_2}(100) \sim 92.5 \times 10^{-15}\ yr\ W\ m^{-2}\ kg_{CO_2}^{-1}$$

It follows that $AGWP_{CO_2}(100) \times t_{yr} \times S_{Earth} = 1.49 \times 10^{9}\ [J\ kg_{CO_2}^{-1}]$ taking into account the unit conversion of $AGWP_{CO_2}(100)$ from $yr\ Wm^{-2}kg_{CO_2}^{-1}$ to $sec.Wm^{-2}kg_{CO_2}^{-1}$. Therefore, $CO_2e\ [kg_{CO_2}]$ in Equation 56 can be rewritten as

$$CO_2e\left[kg_{CO_2}\right] = \frac{(ERF/RF) \times EF_{contrail}[J]}{1.49 \times 10^9 \left[J\ kg_{CO_2}^{-1}\right]} \quad (57)$$

f. nvPM emissions modelling

7.4.43 |The number of non-volatile particulates produced per kg of fuel burn (subsequently referred to nvPM number) is an important engine emissions parameter for aeroengines, as the particulates provide condensation sites for liquid water to then freeze into ice crystals, which make up contrails. The default modelling approach within *pycontrails* is outlined below. It uses engine specific data taken from using the ICAO EDB database[23]. The engine data comprises of nvPM number readings taken at different fuel flow rates. It would not be accurate to estimate the nvPM of an aircraft in cruise by interpolating these fuel flow rates, as those measurements were taken on a stationary aircraft (or test bed) and so inlet flow conditions are different from those for operational aircraft (Teoh and Stettler, 2023; Cumpsty and Heyes, 2015). The non-dimensional quantity T_{04}/T_{02}[24] provides a better parameter for the state of the engine (Teoh and Stettler, 2023; Cumpsty and Heyes, 2015), and thus interpolation should be carried out using this quantity. The equations below enable calculation for fuel flow rates at cruise. First the stagnation quantities at the compressor inlet are calculated by their definitions:

$$T_{02} = T_{amb}\left(1 + \frac{\gamma - 1}{2}M^2\right) \quad (58)$$

$$p_{02} = p_{amb}\left(1 + \frac{\gamma - 1}{2}M^2\right)^{\frac{\gamma}{\gamma - 1}} \quad (59)$$

Stagnation temperatures, T_0, are related to the total energy of the flow at that point (with contributions from thermal and kinetic energy), and stagnation pressures, p_0, are equal to the static pressure of the flow if it was slowed down to rest in an isentropic fashion (no change in entropy). The Mach number is calculated as

$$M = \frac{V}{\sqrt{\gamma RT}} \quad (60)$$

where the true airspeed, V, is found from the difference in the timesteps between each waypoint inputted into the program and by accounting for the local wind speed.

7.4.44 |Combustor conditions are estimated by assuming a linear relationship between the thrust setting, TS, and the combustor inlet stagnation pressure[25]:

$$p_{03} = p_{02}(r_p - 1)(TS) + p_{02} \quad (61)$$

The thrust setting is defined as the equivalent fuel flow rate at sea level over the maximum fuel flow rate. The equivalent fuel flow rate at sea level is

[23] https://www.easa.europa.eu/en/domains/environment/icao-aircraft-engine-emissions-databank
[24] Where T_{04} is the turbine inlet stagnation temperature, and T_{02} the compressor inlet stagnation temperature.
[25] See references in *pycontrails/pycontrails/physics/jet.py* on the *pycontrails* github (Shapiro *et al.*, 2023).

estimated from the cruise fuel flow rate via a conversion given by DuBois and Paynter (2006).

With this in hand, and using the (polytropic) efficiency estimate of the compressor (taken as 0.9 in the model), the stagnation temperature at the combustor inlet, T_{03}, is established as

$$T_{03} = T_{02}\left(\frac{p_{03}}{p_{02}}\right)^{\frac{\gamma-1}{\gamma\eta_c}}. \quad (62)$$

The turbine inlet temperature is then calculated using energy conservation:

$$T_{04} = \frac{AFR\left(c_p T_{03}\right) + q_{fuel}}{c_{p_{comb}}(1+AFR)} \quad (63)$$

7.4.45 |where AFR is the air to fuel ratio, c_p is the specific heat capacity of air, $c_{p_{comb}}$ the specific heat capacity of the combustion products, and q_{fuel} the heat release from burning the fuel. This final parameter is a function of the SAF blend of the fuel (Section 13.6). When nvPM data is not available, nvPM mass and number values are estimated by using the model of a single annular combustor. The nvPM mass number is estimated using the Formation and Oxidation Method (FOX, Stettler *et al.* 2013) and 'Improved' Formation and Oxidation Method (ImFOX, Abrahamson *et al.* 2016), and this is fed into the Fractal Aggregates model (Teoh *et al.* 2019) which estimates the nvPM number. Finally, if this is not possible a default value of $10^{15}\ kg^{-1}$ is used. The models used are developed from multiple sources and use many constants[26]. A number of the engine parameters taken as an input for the nvPM calculations are given in Appendix 1.

7.4.46 |As discussed in Section 13.6, the use of a SAF blend reduces the nvPM emissions from an engine. Equation (75) is provided to scale the nvPM calculations in light of this.

g. Aircraft performance modelling

7.4.47 |The fuel flow rate enters into Equations (2) and (3) by impacting the amount of water vapour and number of soot particles released by the aircraft. The dependence of the water vapour release rate on the fuel mass flow is illustrated in Figure 5 below.

[26] These models can be viewed on the open-access *pycontrails* code repository: https://github.com/contrailcirrus/pycontrails/tree/main/pycontrails/models/emissions

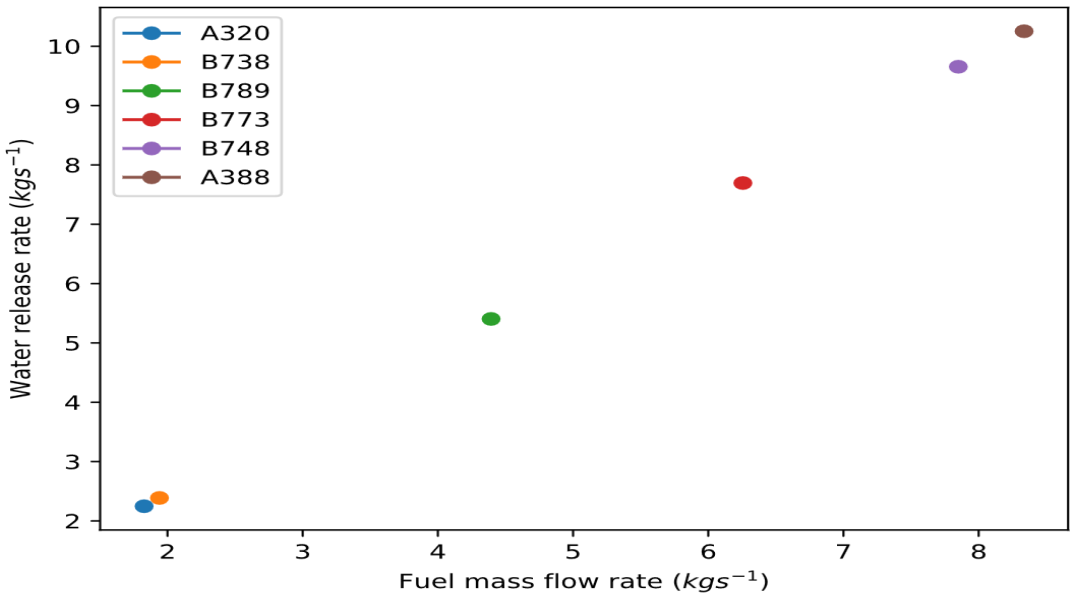

Figure 5 : Rate of water vapour released for the default engine types, set in pycontrails, for specific aircraft, summing over all engines, at 80% of the maximum fuel flow rate.

7.4.48 |The method for modelling the fuel flow for the pre-flight and post-flight analysis is described here.

Pre-flight

- Pre-flight, airlines may supply estimated fuel burn data in the original OFP for use in forecast modelling.

Post-flight

- In a post-flight analysis with ADS-B or GPS tracking data, airline fuel flow data (available in e.g. Quick Access Recorder, QAR, data) will be used if supplied.
- If no data is supplied, the Poll-Schumann model (Section 7.4.50), which takes the tracking data as an input, will be used through *pycontrails* to estimate the aircraft fuel burn throughout the flight. To improve confidence in the fuel flow for a given contrail segment, the fuel flow at all points in the flight, as calculated by the Poll-Schumann model, should be scaled by a scale factor, s, defined as the ratio of the total fuel burn estimate in the modified OFP ($M_{f_{Mod\ OFP}}$) to the Poll-Schumann model's total fuel burn estimate ($M_{f_{PS}}$).

  This method must be slightly tweaked when the Poll-Schumann model cannot be applied at the start or end of the flight. ADS-B occasionally exhibits data gaps along flight trajectories. *pycontrails* can interpolate through these gaps. However, this becomes more challenging if the gaps are at the start or end of the flight, because there are no data points to interpolate between. In these scenarios the scaling factor s should be calculated based off the fuel burn estimates (M_f) over the same sections of the flight.

Therefore if these gaps are such that either the first or last ADS-B datapoint has an altitude > 500ft, the ADS-B data will be trimmed so that either the first datapoint is at approximately the altitude of the first waypoint after take-off, or the final datapoint approximately at the altitude of the final waypoint before landing (or both if required).[27] $M_{f_{Mod\ OFP}}$ should then be calculated as the fuel burnt between the waypoints considered.

The aircraft mass in the Poll-Schumann simulation should be initialised as the take-off mass minus the fuel burn modelled to be burned in any initial waypoints of the modified OFP not covered in the Poll-Schumann analysis.

7.4.49 |The Poll-Schumann model, an open-source aircraft performance model within *pycontrails,* is described below. A list of inputs into the model is provided in Appendix 2. Poll and Schumann have released two papers (Poll and Schumann, 2021a, b) describing an aircraft performance model. The model in *pycontrails* is a more recent version[28], which does not assume the aircraft is at cruise conditions, unlike the papers. This updated version, as implemented in *pycontrails*, is described here.

The ultimate aim of the Poll-Schumann model in *pycontrails* is to estimate the fuel flow rate. This impacts the number of soot particles and the amount of water vapour released. The latter is set in *pycontrails* to be directly proportional to the fuel flow rate, as illustrated in Figure 5.

Fuel flow rate depends on key variables including the lift to drag ratio and the overall efficiency of the engines:

$$\dot{m}_f = \frac{F_{thrust} V}{Q_{fuel} \eta_0} \tag{64}$$

Q_{fuel} is a constant, and the true airspeed, V, is found from the input trajectory's timestamps and the local wind conditions. The thrust force is evaluated as

$$F_{thrust} = mgcos\theta \left(\frac{C_D}{C_L}\right) + mgsin\theta + m\frac{dV}{dt} \tag{65}$$

where θ is the trajectory flight angle (the angle of the incident air, not the angle of attack). In this equation, it is assumed that the aircraft's weight is equal to the lift so that the rate of climb is approximated as constant. As a way to identify key variables, it is noted that when the aircraft is at cruise and at constant airspeed, and when θ is sufficiently small so that the second term can be neglected, that F_{thrust} is directly proportional to C_D/C_L, equivalent to the drag to lift ratio. Substituting this into the equation for $\dot{m}_f$ above shows F_{thrust} to be inversely proportional to $\eta_0 C_L/C_D$. This quantity is known as the range parameter (Poll and Schumann, 2021a) and is key for the aircraft's fuel efficiency.

[27] If the ADS-B data has gaps large enough such that these altitudes are not in the dataset, the second waypoint after take-off, and the second to last datapoint before landing, should be used instead.
[28] From personal communication with Ian Poll.

7.4.50 |Evaluating F_{thrust} requires estimating the lift and drag coefficients. The drag is made up of three main contributions: zero lift drag, lift dependent drag, and wave drag.

$$C_D = C_{D_{zero\ lift}} + C_{D_{lift\ dependent}} + C_{D_{wave}} \tag{67}$$

These calculations depend on aircraft specific parameters which are input into the Poll-Schumann model. The lift coefficient is calculated by equating the lift force to the weight (and accounting for the incidence), and evaluating its denominator, which establishes a non-dimensional lift force:

$$C_L = \frac{mgcos(\theta)}{\frac{\gamma}{2}pM^2S} \tag{68}$$

Combining these values gives the lift to drag ratio.

This leaves the overall engine efficiency, η_0, as the other key factor affecting the fuel flow rate. This depends on the thermodynamic performance of the engine cycle, including the efficiencies of the compressor and turbine, and how well the engine performance is matched to the flight speed (efficiency drops as the difference between the exhaust jet velocity and the flight speed increases). *pycontrails* uses a function which maps the ratio of η_0 to its optimum for a given Mach number (η_0/η_{0_B}), to the ratio of the thrust coefficient of the engine, C_t, to its optimum for a given Mach number (C_t/C_{t_B}). Using this relationship, which is treated as independent of aircraft type, once the ratio (C_t/C_{t_B}) is found, the current engine overall efficiency, η_0, is calculated by multiplying by η_{0_B}. η_{0_B} is modelled using the following power law (Poll and Schumann, 2021b), with the two constants η_1 and η_2, a function of aircraft type in *pycontrails*.

$$\eta_{0_B} = \eta_1 M_\infty^{\eta_2} \tag{69}$$

The thrust coefficient, C_t, is the non-dimensional thrust of the aircraft, defined as

$$C_t = \frac{F_{thrust}}{\frac{1}{2}\gamma pM^2S}, \tag{70}$$

where F_{thrust} is defined above. C_{t_B} is calculated in a similar way as η_0, as

$$TOM = OEM + PM + FM_{nc} + TFM \tag{71}$$

where OEM is the aircraft operating empty weight, PM the payload mass (equal to $load\ factor \times maximum\ payload\ mass$, where the $load\ factor$ is either given as an input or set to 0.7), FM_{nc} is the mass of fuel unused and TFM is the total fuel burn. Payload mass is equal to $load\ factor \times maximum\ payload\ mass$, where the $load\ factor$ includes both cargo and passengers (self-loading cargo) and is either given as an input or set to 0.7. As seen in the equations for F_{thrust} and $\dot{m}_f$, the weight of the aircraft affects the fuel burn at every flight segment. Therefore, iteration is required for an estimate of the TOM, which is done 3 times for each flight in pycontrails. FM_{nc} is estimated by taking the larger of the fuel required to fly at cruise altitude for a further 90 minutes, and an increase in total fuel consumption by 15%

(thus it may change with each iteration). The airline may provide aircraft take-off masses before and after alterations recommended for contrail management, which could be used as an input instead of running the *pycontrails* iterations.

7.5 | Application of downward adjustment

Not Applicable as this is not a GSVER methodology.

8| ACTIVITY EMISSIONS

8.1 | Calculation of total activity emissions

8.1.1 | The project scenario, in the ideal case after re-routing, produces zero net RF from contrail clouds as contrail formation is avoided through the vertical rerouting of the aircraft to altitudes where no contrails are predicted to be able to form. The consequent reduction in climate impact is calculated by comparing the baseline filed flight plan trajectory with the modified flight plan trajectory as attested to by real flown flight path data (using aircraft tracking ADS-B data), coupled to contrail climate impact modelling to calculate radiative forcing associated with both baseline and modified flight trajectories.

8.1.2 | Due to flight operations constraints (e.g., aircraft altitude restrictions and other air traffic control factors), it is not always possible to completely avoid contrail-forming regions by flying modified flight plans as suggested by the project developer/project practitioner. In this case, the project emissions are derived using the same methodology as under the baseline scenario, again using the real flown flight path (however divergent from the modified flight plan).

8.1.3 | Emissions additional to CO_{2e} from contrails, as in 3.2, are still present under the project scenario.

8.2 | Increased emissions

8.2.1 | In changing flight level to avoid contrail-forming regions, aircraft may operate at non-optimal performance which could lead to additional fuel consumption and associated direct emissions (Section 9.1). Fuel burn associated with contrail management is minimal when the approach is fully scaled, with Teoh et al. (2020) calculating a fleet-wide fuel burn increase of 0.014% to reduce contrail climate impact by ~60%. As with the climate impacts of high-performance-compute, additional fuel burn emissions shall be deducted from net climate benefit claims made with regard to contrail management activity. This can be done on a per-flight basis as well as on an aggregated basis (e.g. net climate benefit per larger number of flights or per time period such as quarter or year). The aggregated approach is preferable on a climate accounting basis, since it takes proper account of additional fuel burn arising from incorrect deviations as well as additional fuel burn arising from correct deviations. In turn, given the methodology requirement for an annualized inventory of non-CO2 impact declared by aircraft operators (Section 3.3.6), time period (quarter and/or year) is preferred to number of flights.

8.2.2 | The method for accounting for a fuel burn penalty from contrail avoidance is given in Section 5.2.13.

9| LEAKAGE EMISSIONS

9.1 | Identification of leakage emission sources

9.1.1 | Rerouting of individual flights comes with the potential of other aircraft flying through the original, high contrail propensity airspace which they otherwise might not have been able to access due to traffic concerns (if air traffic management does not include contrail management as a priority). In such cases, climate impact from contrails could still be generated despite individual flights being rerouted. For this to count as leakage, backfill aircraft would need to transverse the same 3-D space as the baseline OFP at a similar time (within <60 seconds).

9.1.2 | In addition to 'backfill' leakage (as described above in Section 9.1.1), a contrail's radiative forcing may potentially be affected by the presence of another contrail. There are two different mechanisms which may cause this type of leakage:

1. A contrail can physically overlap and merge/mingle with pre-existing contrail cirrus cloud.
2. A contrail can, although physically separated, overlap in the vertical with another contrail and affect upwards and downwards radiative fluxes.

9.1.3 | Regarding the first mechanism, there are two possible scenarios: (i) clustering of persistent contrails in heavy air-traffic regions, and (ii) longitudinal overlap of contrails due to two or more aircraft flying on the same trajectory in quick succession.

9.1.4 | Contrail clustering has been studied in the literature to a limited extent (e.g. Bock and Burkhardt, 2016; Duda *et al*., 2001), but it is unclear whether, or how, the radiative forcing of a cluster embedded contrail differs from that of a contrail evolving individually from other contrails. Moreover, although from a ground-based observation contrails may appear to be mixing, in reality they may not be.

9.1.5 | The prevalence of contrail longitudinal overlap is not quantified in the literature, but occurrence is unlikely because aircraft typically avoid flying in the same airmass. Due to safety issues (e.g. wake turbulence), successive aircraft must respect a minimum separation distance when flying on the same trajectory. Moreover, contrails generated by successive aircraft cruising at the same altitude are also unlikely to co-occur in precisely the same airmass because of rapid changes in wind speed and direction (wind shear) in the upper troposphere. High wind speeds (sometimes reaching as high as 200km/hr) perpendicular to the flight trajectory would most likely advect newly formed contrails away from the flight path before the passage of any subsequent aircraft.

9.1.6 | The radiative forcing of contrails formed in the vicinity of each other has been investigated in the context of formation flight (Unterstrasser, 2020), a strategy which can improve aircraft aerodynamic efficiency and whose applicability to commercial aviation has been studied in the recent literature (Khan *et al*., 2023; Tait *et al*., 2022). Inspired from migratory birds, formation flight consists in flying one or more aircraft through another aircraft's wake, with lateral distances ranging from 10%-span overlap to 30 metres separation. Unterstrasser (2020) found that formation flight may significantly reduce the net contrail climate effect in regions conducive to persistent contrails, because contrails generated in close proximity to each other compete for available water vapour, thereby mutually inhibiting their growth. Whilst successive aircraft will not fly as close as in the formation case, longitudinal overlap of their respective contrails may be possible in atmospheric regions of low wind speed.

9.1.7 | Due to the lack of data available on contrail clustering, and the unlikeliness of occurrence of contrail longitudinal overlap, these effects are not quantified or included in the methodology. Contrail prediction models like *pycontrails* are designed to provide a rapid estimate of contrail climate impact and have limitations. Such models are informed by ambient meteorology to simulate contrails, but the coupling is one-way, meaning there is no feedback between the simulated contrails and the ambient atmosphere. Therefore, *pycontrails* cannot provide information on how contrails may impact their surroundings, including other contrails.

9.1.8 | The second mechanism (contrail vertical overlap) has been investigated in the literature. Sanz-Morère et al. (2021), in a study of 2015 aircraft flight data, calculated a 3% radiative forcing reduction resulting from contrail-contrail vertical overlap. The authors note that there is large uncertainty in this estimate through its dependence on average contrail optical depth. A more recent study investigating the effects of contrail vertical overlap estimated a reduction in the annual mean contrail net RF by 5% globally, and by 9.4% over Europe due to the high density of air traffic (Teoh et al., 2024). A limitation of both studies is the assumption of maximum vertical overlap between contrails inside a given horizontal grid cell. Due to the highly dynamic nature of the upper troposphere (i.e. wind shear, turbulence), full vertical overlap of contrails is usually of very short duration. A relaxation of this assumption is likely to cause a drop in the predicted RF reduction and indicates a need for further work in this area.

9.1.9 | Further investigation needs to be undertaken across academia and the industry to quantify the prevalence and impact of contrail merging and overlap. If future research substantiates that these effects cause significant changes to contrail net radiative forcing, then the calculated climate impact shall be adjusted accordingly. For example, where in retrospective (hindcast) analysis it is determined that contrail vertical overlap occurred, the calculation of contrail radiative forcing should follow the conservative method described in Teoh et al., 2024.

9.1.10 |The possible leakages described above have high levels of uncertainty but are unlikely to be material in the near term. They are therefore not included in quantification in this methodology. The possible leakage sources will be reviewed by the end of the first crediting period or by 31 December 2030, whichever comes first. If any of these leakages are estimated as material, they shall be quantified and included thereafter.

10| CALCULATION OF MITIGATION OUTCOME

10.1 | Calculation of mitigation outcome

10.1.1 |Since calculations are undertaken post-flight, and there is an option for project practitioners to run an NWP in hindcast mode if they have found it to be significantly more accurate than a forecast (e.g. > 10% more accurate in F1 score or alternative key metric for forecast skill of relative humidity). Reductions in emissions can be calculated on a per flight basis, using multiple implementations of the detailed model workflow (see 3.1).

a. A CO_2e impact is first calculated for the 'baseline' operator flight plan (OFP), i.e. the OFP that would have been flown without any modifications for the purpose of contrail management.

b. A CO_2e impact is retrospectively calculated for the OFP plan that was modified (optimised) for contrail prevention. The difference in CO_2e between this OFP and the unmodified OFP is the estimated potential net CO_2e saving.

c. A further calculation of CO_2e is performed using the actual flown flight path as given by GPS or ADS-B data, enabling the actual net CO_2e saving, in comparison to the unmodified OFP, to be calculated.

d. The change in fuel burned resulting from contrail management, ΔM_f, will be estimated as the difference between the total fuel burn in the modified OFP and the total fuel burn in the baseline OFP. This enables the fuel burn penalty (if present) of contrail management to be accurately estimated and avoids applying a penalty for operational changes made during the flight.

10.1.2 |In order for the fuel burn comparison between the OFPs to be valid, any variables inside the flight planning software which impact the fuel burn of an aircraft (for example the load factor, or weather parameters like wind speed) must be the same other than those changed as a result of planned contrail management. Therefore, in the delivery process, if in the time elapsed between generating the baseline OFP and preparing the modified OFP (after receiving contrail management guidance from e.g. GE Aerospace's Aerospace Carbon Solutions), these variables have changed, the baseline OFP should be re-run just prior to generating the modified OFP. Both OFPs should then be sent to the project practitioners, who should check that the specified load is the same, and that the same weather inputs have been utilised both for original and modified OFPs. The mitigation outcome which can be claimed, for a given reporting period, y, can thus be calculated as

$$CMO_y = \sum_{i=1}^{F} BE_i - PE_i - L_i \quad (72)$$

11| MEETING METHODOLOGICAL PRINCIPLES

11.1 | Avoidance of double counting

11.1.1 |To mitigate the risk of double issuance and claims, the project developer shall conform with the requirements and apply the procedures set forth in the GHG Emissions Reduction & Sequestration Product Requirements that no double-counting takes place.

12| REVERSALS

12.1.1 |Not applicable.

13| QUANTIFICATION OF UNCERTAINTY

13.1.1 |An initial indication of the general accuracy of CoCiP, as implemented in *pycontrails*, comes from a global estimate of contrail radiative forcing (RF) undertaken by Teoh *et al*. (2024), utilising the BADA aircraft performance model rather than the Poll-Schumann model. Using a year's worth of flight tracking data and reanalysis weather data from ECMWF as inputs to CoCiP, they estimated a global mean contrail net RF of $62.1\ mWm^{-2}$ for 2019 with a range of $34.8 - 74.8\ mWm^{-2}$.

13.1.2 |Prior to Teoh *et al*. (2024), Lee *et al*. (2021), estimated the total forcing for 2018 by scaling the results of four different global model studies of contrail forcing; one of these, Schumann *et al*., 2015, used the CoCiP model in a different implementation to *pycontrails*. The mean value obtained was $111\ mWm^{-2}$ with a 5–95% confidence range of $33 - 189\ mWm^{-2}$ estimated by considering the uncertainties associated with modelling of the different relevant physical processes. The range in global contrail net RF estimated by Teoh *et al*. (2024) therefore fits within the range calculated by Lee *et al*. (2021); while this new estimate improves confidence in the magnitude of the RF for a very large number of flights, the exact magnitude of the energy forcing for individual contrails remains uncertain.

13.1.3 |The uncertainty around the calculated contrail energy forcing $(EF_{contrail})$ for a given flight can be largely attributed to three sources:

(i) uncertainty in numerical weather prediction (NWP)

(ii) uncertainty in CoCiP/*pycontrails*

(iii) uncertainty in converting $EF_{contrail}$ to CO_2e

13.2 | Uncertainty in NWP

13.2.1 |Relative humidity with respect to ice (RH_{ice}) of the ambient atmosphere is a critical variable for determining contrail lifetime: if RH_{ice} is greater than 100%

within the contrail, the specific humidity within is above saturation (Section 7.4.23, Equation (31), $q_a - q_s > 0$)) and the model will deposit water vapour onto ice crystals. RH_{ice} is a function of specific humidity, temperature, and pressure:

$$RH_{ice} = \frac{q}{q_s(p,T)} \quad (73)$$

13.2.2 |There is consensus in scientific literature that uncertainty in contrail RF estimates is dominated by uncertainty in predicted RH_{ice} at cruise altitude (Schumann, 2012; Schumann *et al*., 2021; Teoh *et al*., 2022). In a CoCiP model experiment, Schumann *et al*. (2021) found that varying RH_{ice} by 5% changed contrail net RF in the order of 60%. Teoh *et al*. (2022) found that applying corrections to humidity fields from the ERA5 reanalysis caused simulated contrail cirrus net RF to drop by 49%. More recently, Teoh *et al*. (2024) assessed *pycontrails* sensitivity by calculating global estimates of contrail net RF when modelling or not modelling certain processes. The analysis revealed that the simulated contrail net RF is most sensitive to corrections applied to predicted humidity fields, corroborating findings from previous studies.

13.2.3 |Extensive scientific validation has been performed by SATAVIA on the water vapour predictions created by WRF. Over time the skill of this and other NWP models will improve, reducing levels of uncertainty associated with the outcome of deviations done to avoid the warming caused by contrails. Future claims and issuances may be adjusted down to account for ISSR prediction and contrail modelling uncertainty, in line with best available scientific evidence regarding relevant uncertainties. In addition, further scientific activity can be carried out to quantify potential leakage effects caused by intermingled contrails and by interactions with natural clouds.

13.2.4 |While NWP weather models are mostly accurate in their prediction of atmospheric pressure, errors in specific humidity and temperature forecasts can be significant. The quality of numerical weather predictions is routinely assessed by retrospectively comparing the weather forecasts against observational data to generate statistics on model forecast skill[29].

[29] Note: SATAVIA has recently evaluated the Weather Research and Forecasting NWP model, WRF, as well as two leading global NWP models (Global Forecast System, GFS, and the Integrated Forecast System, IFS), in the ability to predict ISSR (RH_{ice} ≥ 100%) at aircraft cruise altitudes (Thompson et al., 2024). Water vapour parameters calculated by the NWP models were evaluated against radiosonde and aircraft in situ measurements over Europe and the Middle East for 10 months in 2022. The models' predictive skill was first measured in terms of prediction bias/error for various atmospheric parameters (e.g. temperature, water vapour, RH_{ice}). The skill of the models is closely related to the nature of the cloud microphysical scheme used (i.e., multi-moment scheme to explicitly account for the characteristics and evolution of the hydrometeors formed) and model spatiotemporal configuration.

13.2.5 |Statistics can be generated that describe the ability of a NWP model to forecast ISSR, which can be used to assess the viability of navigational avoidance of warming persistent contrail-forming conditions. The analysis presented in Thompson *et al.* (2024) revealed that, despite being imperfect in their prediction of ISSR, NWP models have reached sufficient skill today on balance to provide a net climate mitigation across a cohort of flights. The benefit arising from preventing persistent contrail formation outweighs (by several orders of magnitude in terms of CO_2e warming) the combined impact of penalty emissions and erroneous rerouting of aircraft into ISSR (Thompson *et al*., 2024).

13.2.6 |Of particular note, another recent study by Akhtar Martinez and Jarrett (2024) investigated the trade-off between additional fuel burn and avoided contrail climate impact by propagating uncertainty in weather inputs through two different contrail models, one of them being *pycontrails*. The authors estimated that contrail climate impact models need to be at least 65% accurate to be used for contrail avoidance, thus highlighting the fact that, even with a non-negligible degree of uncertainty in their inputs, such models can drive successful contrail mitigation.

13.3 | Uncertainty in CoCiP/pycontrails

I. Model internal assumptions/parameters

13.3.1 |Like many deterministic models, pycontrails relies on assumptions, physical constants, and empirical coefficients – like those listed in Annex 3 – to describe the behaviour of the system under consideration. If these parameters are poorly constrained or inaccurately calibrated, errors can arise which can introduce significant uncertainty into the model's predictions.

13.3.2 |Sensitivity analyses can be designed to measure the response of the contrail prediction model to various inputs and tuneable internal parameters. The method consists in systematically varying the parameters by running the deterministic model many times, each time with a different value for a given parameter or set of parameters. Based on available information, the possible values assigned to these parameters can be guided either by observational data, or by values published in the literature or, if neither of the previous options are available, by a percentage of the default value.

13.3.3 |Previous published sensitivity analyses have shown how CoCiP/pycontrails' output radiative forcing varies due to varying inputs and internal parameters (Platt et al., 2024; Teoh et al., 2024; Teoh et al., 2022). The second most important factor, after RH_{ice}, is the number of emitted particles that nucleate into ice crystals, followed by the NWP input shortwave and longwave radiative forcing. The radiative forcing data has a large influence for the same reason as the RHice, since the NWP model may have existing clouds at various altitudes that directly affect the total contribution of the contrail's radiative forcing.

Other internal parameters that merit investigation include:

- Integration time step

- Ice terminal velocity, indirectly tested through the sedimentation impact factor, f_T (Equation 25): a scaling factor for the contribution of sedimentation to the vertical diffusivity coefficient, D_V
- Radiation scattering by ice particles of different ice habit/geometry
- Pre-existing/ambient aerosols (especially dust and sulfates) that can act as ice nuclei
- Wind shear enhancement factor, f_s (Equation 28): a scaling factor for the estimated total wind shear, which enters into the calculations for horizontal diffusivity, D_H
- Initial wake vortex depth, C_{D0} (Equation 7): a scaling factor applied to the calculated maximum downwash to define the initial depth of the contrail

13.3.4 |A Sobol method, a variance-based Global Sensitivity Analysis (GSA), can be used to rank the relative importance of the parameters. The primary uncertain parameters within CoCiP/pycontrails can then be incorporated into a probabilistic risk management method as discussed in Section 13.5.1.

II. Engine emissions

13.3.5 | It is emphasized that CoCiP is a Lagrangian plume model that starts its simulation at the down wash step – this is a jet engine plume that has already aged minutes after emission from the engine. Early plume physics and chemistry involving ice nucleation particles (INPs) simply are not simulated. Early ice particles formed in the jet regime, passing through the vortex regime and within the dissipation regime, have already completed; this is the starting state of CoCiP simulation.

13.3.6 |The microphysics in the early plume phase can be simulated by other models such as the Advanced Particle Microphysics (APM) model as initially detailed by Yu and updated and referred to as the Aerosol and Contrail Microphysics (ACM) Model (Yu *et al.*, 2024). More complex models can be run as a pre-model input step to CoCiP to provide better input to CoCiP at the down wash step or simply be used as a guide for better CoCiP model input.

To realize this, one could approach differences in jet fuel type and engine types and specifically lean burn engines where ice is formed from volatile particulate matter (vPM) rather than soot by pre-assigning the correct number of ice nucleators in these different cases. This can then be assigned within CoCiP for each simulation step.

13.3.7 |While sustainable fuels and lean burn engines are relatively new and further research is needed, there have been a number of experimental studies conducted, and we have some sense of how these impact ice nucleators. While ground based soot measurements of production engines using SAF are not available, experimental flight campaigns may be used for understanding soot emission from sustainable aviation fuels (SAF) fuel types. Specifically, during ECLIF flight campaigns (Le Clercq *et al.*, 2022; Voigt *et al.*, 2021: Märkl *et al.*, 2024) various blends of SAF and Jet-A were studied with subsequent ice particle measurements downstream of the engine. A drop in ice counts (number density) was noted for the different SAF/Jet-A blend fuel

types relative to pure Jet-A that was attributed to lower soot emission intensities. Additionally, the carbon to hydrogen ratio in the different fuels were also noted. These differences will result in different water emission intensities relative to Jet-A that can be used as a variable in CoCiP simulations. For example, the emission intensity of water was reported to increase in 100% HEFA SPK fuel from 1.26 (100% Jet A) to 1.35 kg water/kg fuel burn.

13.3.8 | Lean burn engines represent a fundamentally different engine type relative to standard rich-burn-quench engines. Production engines such as GEnx for widebody aircraft and CFM International LEAP engines for narrowbody aircraft produce orders of magnitude less soot and thus contrail formation must involve a majority of ice nucleation from vPM instead of soot. In the case for ice forming from vPM, again, this can be accounted for by implementing emission intensity estimates of vPM rather than nvPM.

13.3.9 | Unlike nvPM, vPM is not regulated or measured in production engines. Furthermore, it is in only very recent flight campaigns where ice particle measurements have been made of lean burn engines. Flight campaigns from the 2023 VOLCAN-2[30] and 2023 ecoDemonstrator[31] campaigns both used CFM LEAP engines with JetA and SAF fuels. Only preliminary results from these campaigns are available, although contrail formation has been observed - thus demonstrating that vPM as an effective nucleator in contrail formation. Large scatter in the ice count data was observed with a reduction in counts similar to the reduction seen from the use of SAF and SAF blends in rich burn engines.

13.3.10 | Mechanistically, accounting for lean burn engine vPM is straightforward and can be realized in CoCiP by replacing nvPM counts with vPM estimates. Complex chemistry of vPM can be simulated by early plume models and used in conjunction with CoCiP as explained above.

The product development team plans to use chosen ranges in nvPM uncertainty adequately representing the range of ice nucleators from both changes in SAF blends as well as lean burn engines. As an example, measured ice count data from the ECLIF 3 campaign shows a reduction of ice emission intensity of 0.78×10^{15} to 0.34×10^{15} #/kg fuel burn from pure Jet A1 to pure HEFA-SPK fuel.

13.4 | Uncertainty in $EF_{contrail}$ to CO_2e conversion

I. Uncertainty of $\mathbf{AGWP_{CO_2}(100)}$

13.4.1 | We note that there is uncertainty around $AGWP_{CO_2}(100)$ due to different model selection and choice of background scenario. Internal calculations using model coefficients given in Joos et al. (2013), Table 5, resulted in $AGWP_{CO_2}(100) =$

[30] https://www.airbus.com/en/newsroom/stories/2023-03-airbus-most-popular-aircraft-takes-to-the-skies-with-100-sustainable
[31] https://www.boeing.com/sustainability/environment/ecodemonstrator/history#2023

$92.0 \times 10^{-15}\ yr\ W\ m^{-2}\ kg_{CO_2}^{-1}$. The discrepancy between this value and the $AGWP_{CO_2}(100)$ calculated by Joos et al. (2013) is less than 1%. Further internal calculations using a different model, Linclim (Sausen and Schumann, 2000), led to $AGWP_{CO_2}(100) = 97.1 \times 10^{-15}\ yr\ W\ m^{-2}\ kg_{CO_2}^{-1}$. The latest IPCC value, communicated in the IPCC Fifth Assessment Report, 2014 (AR5) WGI, Chapter 8, Table 8.A.1, is $AGWP_{CO_2}(100) = 91.7 \times 10^{-15}\ yr\ Wm^{-2}kg_{CO_2}^{-1}$ (Myhre et al., 2013). More recently, Hodnebrog et al. (2020) communicated an updated value of $AGWP_{CO_2}(100) = 80.6 \times 10^{-15}\ yr\ Wm^{-2}kg_{CO_2}^{-1}$, which is about 14% lower than the AR5 value.

13.4.2 |All four $AGWP_{CO_2}(100)$ values reported here are well within the 95th confidence interval of $AGWP_{CO_2}(100) = 92.5\ [68, 117] \times 10^{-15}\ yr\ Wm^{-2}kg_{CO_2}^{-1}$ given by Joos *et al*. (2013). This confidence interval may be used, with an appropriate sampling distribution to be determined, to quantify how the uncertainty in $AGWP_{CO_2}(100)$ impacts CO_2e.

II. Uncertainty of **ERF**/**RF** ratio

13.4.3 |Lee et al. (2021), recommend a global ERF/RF ratio of 0.42 for the computation of contrail effective radiative forcing. This value is an average of ERF/RF ratios from three different research papers, $0.59, 0.31$ and 0.35, respectively (Ponater et al., 2005; Rap et al., 2010; Bickel et al., 2020). There are two more recent studies (Bickel et al., 2025) with normalized ERF/RF of 0.42 and 0.55. Including these two results in the average of 5 values results in 0.44. We adopt this global ERF/RF ratio in our calculation.

13.4.4 |Given the current limited research studies available on ERF/RF ratio for contrails, one way to quantify the uncertainty of this ratio is to derive volatility from the five values known in the literature with an appropriate sampling distribution to be determined.

13.4.5 |Moreover, the ERF/RF ratio we adopt from Lee *et al*. (2021) is a global ratio; regional ERF/RF ratios for individual contrails are not available in any study yet. In summary, further research is needed to derive a more precise ERF/RF ratio for individual contrails.

III. Uncertainty of contrail **EF** for single flight

13.4.6 |The uncertainty of $EF_{contrail}$ in the nominator of Equation 56 may be quantified by means of a Monte Carlo analysis.

13.4.7 |On the other hand, given a $EF_{contrail}$ with uncertainty from one single flight, one way to reduce the uncertainty is to consider EF from multiple flights from a statistical aspect, for example, by considering CO_2e contrail on daily basis or by certain region or by operator.

IV. Uncertainty around time evolution of contrail **RF**

13.4.8 |Borella et al. (2024) applied a reduced complexity earth system (OSCAR) model with carbon cycle feedback process adjustment to simulate the time evolution of contrail radiative forcing. The time evolution of the contrail radiative forcing years after contrail formation is not considered in our model but may be considered in our future research.

13.5 | Strategy to deal with uncertainty: mitigating risk and Operating Characteristic (OC) curves

13.5.1 |A notionally simple model chain that can be evaluated to calculate the expected value of CO2e for a flight path is shown in Figure 6 In this model chain, we consider three models, namely:

a) Numerical Weather Prediction Model (NWP),

b) Physics-based contrail lifetime simulators (here *pycontrails*), and

c) $\mathrm{EF}_{\mathrm{contrail}}$ to CO_2e conversion.

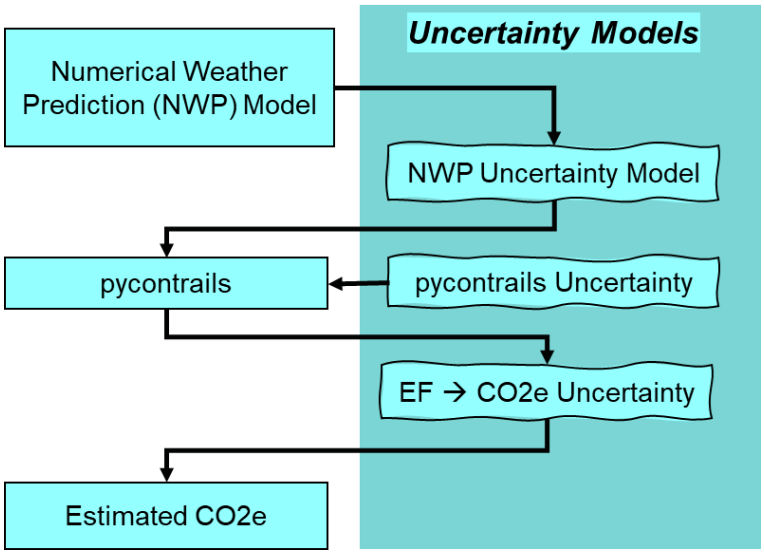

Figure 6 : Model chain considered in uncertainty quantification (UQ) methodology

13.5.2 |As discussed in Section 13.2.4 |, the NWP prediction of RH_{ice} represents the largest uncertain input to the contrail prediction system. The radiosonde validation study (Thompson et al., 2024) provides an ideal dataset to use directly in the NWP uncertainty model shown in Figure 6. Using the full set of 1.5M error values of S-WRF RH_{ice}, the uncertainty model can use Monte Carlo sampling of those values as offsets from the NWP model data to ascertain the sensitivity in resulting CoCiP radiative forcing (or converted CO_2e value). Through repeated random sampling, a probability of Expected Value can be produced.

13.5.3 |Two techniques of introducing typical NWP model error into CoCiP evolved during the development of this methodology. The first technique used purely random sampling of the error dataset along each waypoint for a series of sample flights. This will be referred to as the "gray noise" ensemble, because the ensemble has no recognizable pattern in a spatial sense. The second technique used a gradient noise scheme attributed to Ken Perlin (1983), which produces smooth pseudo-random noise that mimic real world features or phenomena such as clouds. Perlin noise has also been used in machine learning models to perturb initial conditions to produce ensemble forecasts (Bi *et al*., 2022; Chen *et al*., 2023).

13.5.4 |The parameters of the Perlin noise pattern can be easily adjusted to produce a series of perturbations that align with the error data from the radiosonde study. These patterns represent spatially coherent error values that can be added to predicted relative humidity data, similarly to the gray noise technique. Thus a "Perlin noise" ensemble can similarly output 50 (or more) ensemble values of the radiative forcing of individual contrails.

13.5.5 |An example visual representation of a Perlin noise ensemble is shown in Figure 7, overleaf. The single deterministic NWP areas of ice supersaturated regions (ISSR) are shaded red, while the shades of blue vary depending on the fraction of perturbed ensemble members having an ISSR. This creates a very realistic pattern of typical weather prediction errors, especially when compared to the gray noise ensemble.

13.5.6 |The output of the gray and Perlin noise ensembles of contrail radiative forcings for a sample flight is shown in Figure 8, overleaf. The flight transited from Los Angeles, CA (LAX) to Heathrow, London (LHR), passing through the two regions of ISSR seen in Figure 7. The waypoint-by-waypoint values of radiative forcing show the expected variability due to using perturbed relative humidity data. In general, the gray noise ensemble has less variability than the Perlin noise since the former method produces some cancellation effects of regions switching between ISSR and non-ISSR. The Perlin noise pattern with spatially and temporally correlated perturbations produces an overall larger spread of radiative forcing.

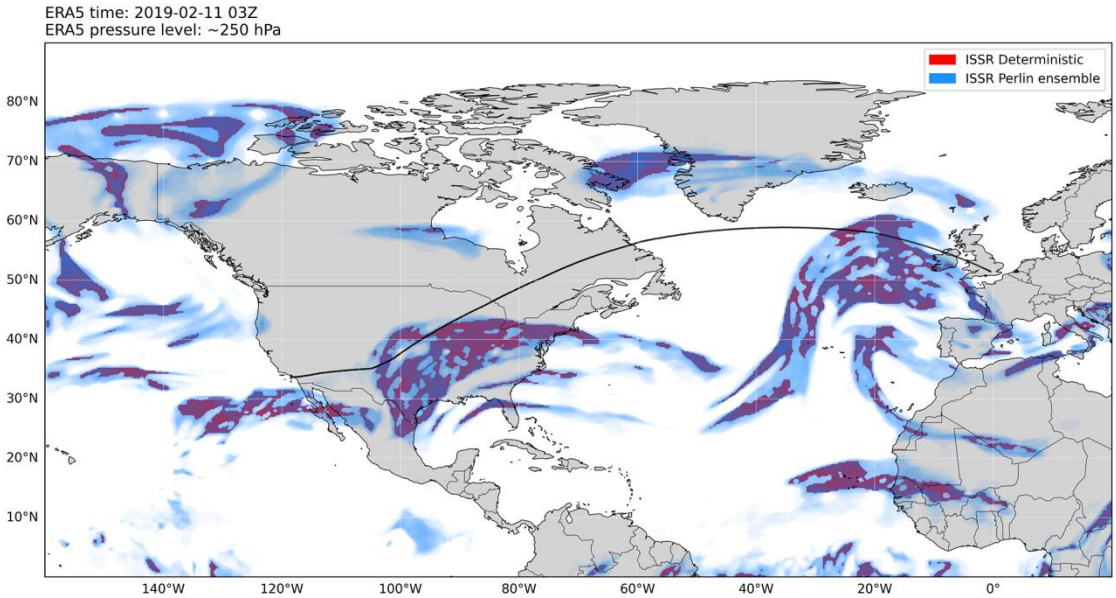

Figure 7 : Perlin noise pattern introduces perturbed RHice values causing shifts in ISSR. The unperturbed NWP data is shown in red and Perlin noise random sampling (size = 50) is depicted in deeper shades of blue as more ensemble members have RHice > 100

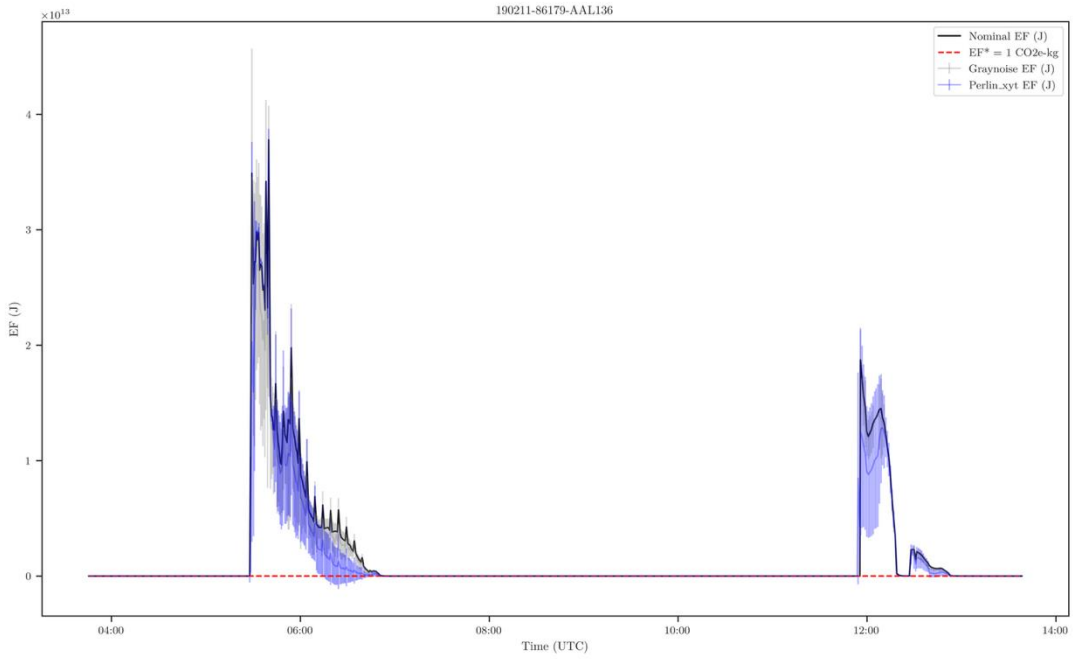

Figure 8 : Example CoCiP radiative forcing from deterministic weather prediction data (black line), gray noise perturbed ensemble (gray lines) and Perlin noise ensemble (blue lines) showing uncertainty in contrail radiative forcing from perturbing the relative humidity data

13.5.7 |As shown in Figure 8, the perturbations by either gray or Perlin noise now generate different values of cumulative radiative forcing for each ensemble member. Figure 9 presents those results in a frequency histogram to show the variability. The output radiative forcing is shown on the bottom axis and the calculated CO_2e is shown on the top axis for this example flight. The unperturbed (or deterministic) value is 386 T, but most of the ensemble members are lower due to the frequent likelihood of weather prediction errors producing fewer overall ISSR conditions.

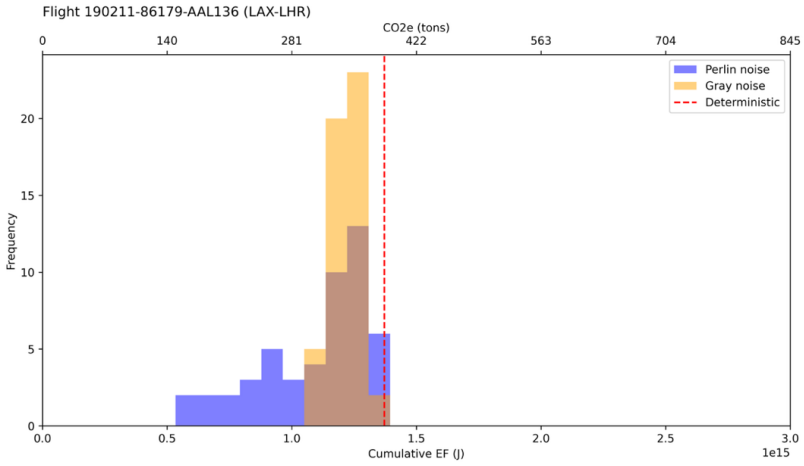

Figure 9: Example frequency distribution of CoCiP cumulative radiative forcing from deterministic weather prediction data (red dotted line), gray noise perturbed ensemble (orange boxes/brown where overlapping with Perlin boxes) and Perlin noise ensemble (blue boxes) for the example flight from LAX to LHR.

13.5.8 |Given either single or multiple sources of uncertain input data, they can be propagated through the model chain to estimate the probability of exceeding a specific amount of CO_2e for any flight. Classically, this is done with an operating characteristic (OC) curve, similar to Figure 10, overleaf. This example only includes the RH_{ice} uncertainty, but any number of additional inputs could be utilised, such as NWP temperature, one or more CoCiP internal parameters, or the conversion factors used to translate CoCiP energy forcing into CO_2e values. Usage of the OC curves is straightforward in that the Perlin ensemble gives a 90% probability that this example flight will reach 200 T of CO_2e, yet gives less than 50% probability that this flight will exceed 330 T. Using the completely uncorrelated gray noise technique produces a 90% likelihood of reaching 310 T CO2e. However, the usage of the purely random perturbations at each waypoint is sub-optimal, since weather prediction errors are highly correlated in space and time.

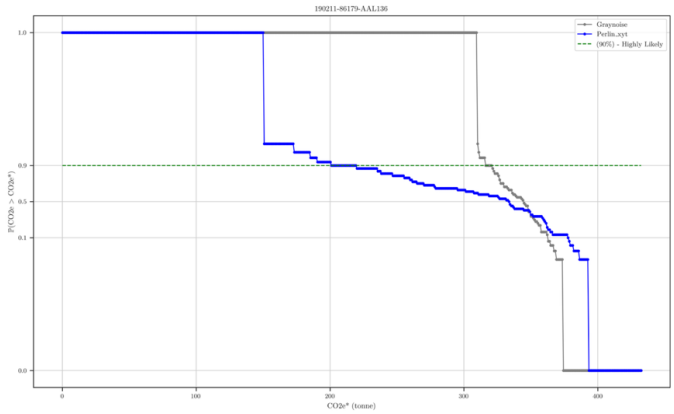

Figure 10 : Example operating characteristic curve showing the probability of exceeding specific values of CO2e from the gray noise (gray line) and Perlin noise (blue line) ensembles for the sample flight from LAX to LHR.

13.5.9 |It is worth highlighting that the quantity in question is firstly the variation in predicted CO_2e of flight trajectories which are modelled to have a high impact, since flight trajectories which are not predicted to a have a high impact will likely not undergo contrail management in the approach outlined in this methodology. Equally important is the uncertainty in the predicted CO_2e of deviated flight trajectories, which will likely have a low modelled impact (or at the very least reduced) compared with the initial flight trajectory.

As an example, the OC curve of a different flight is shown in Figure 11. In this example, there is a 90% likelihood that any contrail it produces will result in approximately 2 T CO2e, which implies the flight is not a very good choice for a diversion. Similarly, this methodology can be readily extended to create a very high confidence in the proposed choice of rerouting. In other words, only when there is a very high likelihood of near-zero CO_2e on the candidate route should a suggested flight plan diversion be provided.

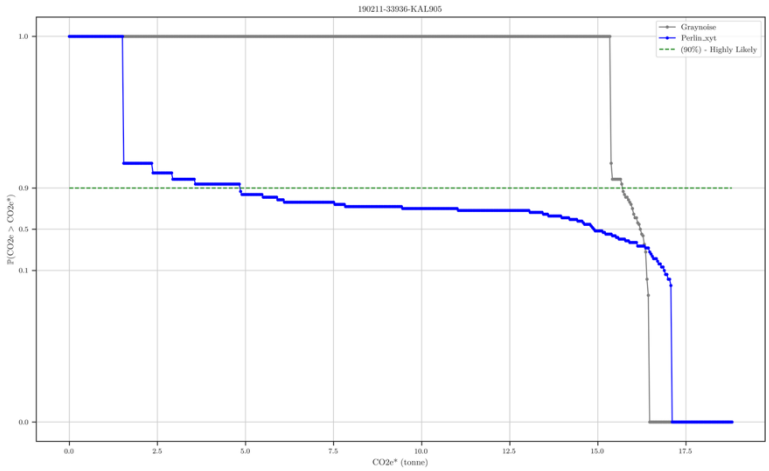

Figure 11 : Operating characteristic curve for an example flight with a very low likelihood of producing more than 2 T CO2e, indicating that this flight should not generally be considered for a diversion to avoid producing a contrail.

13.5.10 | This uncertainty quantification methodology could also be used to decide a specific value of CO_2e to link to CMO issuance. For example, since the unperturbed NWP data is not the most likely outcome when considering various data uncertainties, a statistically more likely value could be linked to the CMO. In the example flight presented in Figure 8, the unperturbed NWP data passed through CoCiP results in 386 T CO_2e, but the Perlin ensemble provides an opportunity to choose a different statistical value. The median value from the ensemble for example flight is 333 T, whereas the 25th percentile value is 266 T and the 5th percentile value is 187 T. The choice of which percentile value to link in creating CMO is a valid discussion point for future iterations of this methodology.

13.5.11 | The methods described above represent initial suggestions for testing sensitivity and quantifying uncertainty of the modelled contrail climate impact, which could inform future weightings of CO_2e calculations for optimised (contrail avoidance) flight plans. Future iterations of this methodology, conducted with transparent version control in line with routine Gold Standard methodology development, implementation and revision procedures, can adopt findings from peer-reviewed research on these and other methods as it becomes available in the field of contrail science. Model changes are less likely to represent dramatic shifts in approach or climate impact than they are to represent incremental improvements arising from (e.g.) new approaches to weather modelling and/or the capacity rapidly to assimilate observational data provided by in-situ aircraft sensors, satellite observations, or both. In any specific crediting period, differences in mitigation outcomes will be due to variations in atmospheric conditions and aircraft configurations rather than to variations in models used.

13.6 | Impact of non-fossil carbon fuels on contrail radiative impact modelling

13.6.1 |Non-fossil carbon fuels, such as Sustainable Aviation Fuel (SAF) and hydrogen, provide future alternatives to conventional Jet A1 kerosene used in

commercial aeroengines. SAF exists in a variety of formulations and is typically made from renewable sources, such as used cooking oil, agricultural waste, or forestry waste. SAF combustion releases similar amounts of CO2 to Jet A1, but typically releases lower amounts of particulate matter, which potentially leads to lower contrail radiative impact by reducing the number of potential nucleation sites which results in a lower number of larger hydrometeors (Voigt et al., 2021). SAF usage currently accounts for <1% global commercial aviation fuel requirements, with scaling expected to be slow (<10% global requirements by 2030); consequently, SAF impact on contrail formation is likely to be limited. Taking account of supply constraints, researchers have suggested blending SAF with Jet A1 on a targeted percentage of flights expected to form the most warming contrails, with estimated reduction in fleet contrail radiative forcing ~10% when supplying ~2% of flights with a 50% SAF blend (Teoh et al., 2022).

13.6.2 |Pycontrails enables a SAF blend of the jet fuel to be set in the model, allowing for fuel-specific calculation of SAF-generated contrail climate impact (rather than, e.g., applying a percentage reduction to contrail climate impact calculated for kerosene Jet A1 contrails). This impacts the following three parameters in the code which are relevant to contrails: the amount of water vapour released; the heat addition from combustion in the engine; and the number of particulates and mass of emitted nvPM. By applying the below adjustments, the impact of SAF can be included in this methodology.

13.6.3 |The water emission index of a SAF blend, $EI_{H_2O_{SB}}$ (the kg of water emitted per kg of fuel burnt) is defined as:

$$EI_{H_2O_{SB}} = EI_{H_2O_{JA1}} \frac{m_{H_{JA1}} + (0.015 \times SB)}{m_{H_{JA1}}} \tag{74}$$

where $EI_{H_2O_{JA1}}$ is the water emission index for Jet A-1 fuel, $m_{H_{JA1}}$ is the percentage of hydrogen in Jet A-1 by mass, and SB is the percentage SAF blend. This equation is taken from Teoh *et al*. (2022). This term is used for initialising the mass of ice in the contrail.

13.6.4 |The heat addition resulting from the combustion of SAF is set as

$$q_{SB} = q_{JA1} + (10700 \times SB) \tag{75}$$

following Teoh *et al*. (2022), Supporting Information, and references within.

The change in the nvPM number emissions is calculated with a dependence on the change in hydrogen mass content of the fuel (Δm_H) to be:

$$\Delta\text{nvPM EI}_\text{n} = \begin{cases} (\alpha_0 + \alpha_1 TS)\Delta m_H, & \Delta m_H \leq 0.5\% \\ (\alpha_0 + \alpha_1 TS)\Delta m_H \times e^{0.5-\Delta m_H}, & \Delta m_H > 0.5\% \end{cases} \tag{76}$$

following Teoh *et al*. (2022). The same equations are applied to evaluate the change in nvPM mass emissions, but with different constants $\boldsymbol{\alpha_0}$ and $\boldsymbol{\alpha_1}$.[32]

[32] https://github.com/contrailcirrus/pycontrails/blob/main/pycontrails/models/emissions/black_carbon.py

14| MONITORING METHODOLOGY

14.1 | Data and parameters not monitored

14.1.1 |In addition to the data and parameters listed in 14.1.4, there are several constants within the contrail climate impact model which are taken from the scientific peer-reviewed literature (e.g., ice habit dependent constants for interaction with radiation). See Annex 3 for more details.

14.1.2 |Airline operators are unlikely to intentionally propose base scenarios where warming contrails are highly likely along the original Operational Flight Plan (OFP), as flight planning software typically generates performance-optimized (i.e., baseline OFP) flight plans automatically, without integrated contrail management intelligence. To prevent gamification, the methodology relies on a stepwise process: first, a baseline OFP is generated using industry-standard flight planning software optimized for traditional factors such as fuel burn, weather, payload, and air traffic control charges. Next, the likelihood of contrail formation along the baseline trajectory is calculated using contrail prediction models. If contrail formation is likely, alternative flight paths above or below the baseline trajectory are evaluated to identify options that reduce contrail formation while maintaining operational feasibility.

Proof of gamification, such as intentional selection of contrail-prone flight paths as baseline scenarios, would lead to the discounting or cancellation of CMO issuance. Immutable distributed ledger technologies, already in use within the project boundaries, provide a mechanism for validation and verification bodies to confirm compliance. For example, metadata generated by flight planning software can be inspected to verify the absence of manual overrides during baseline OFP generation. Additional checks, such as comparison of OFPs to historical trajectory patterns or forecast ISSR regions, can be used to detect anomalous deviations indicative of tampering. Project developers must provide auditable data demonstrating the sequence of baseline OFP generation, contrail likelihood assessment, and subsequent optimization for contrail mitigation to ensure transparency and accountability.

14.1.3 |There exists the potential for air traffic managers to fill the airspace left by a contrail-rerouted flight. Under the current project boundary, only the target flight is monitored.

14.1.4 |The following list details data and parameters not monitored in the current project boundary. In these cases, the variables are estimated using the contrail climate impact model. They are therefore not model inputs, but rather internal variables calculated in every pre and post flight analysis. There are many internal variables in pycontrails – a number of examples are given below.

Parameter ID	DXNZ 1
Data/Parameter:	B
Data unit:	m
Description:	Width of contrail as defined from Gaussian plume.

Source of data:	Contrail evolution model.
Any comment:	To monitor the width of any contrails formed under the project scenario and/or through leakage, high resolution (spatial and temporal) satellite data with global coverage would be required.

Parameter ID	**DXNZ 2**
Data/Parameter:	D
Data unit:	m
Description:	Depth of contrail as defined from Gaussian plume.
Source of data:	Contrail evolution model.
Any comment:	-

Parameter ID	**DXNZ 3**
Data/Parameter:	L
Data unit:	m
Description:	Length of contrail segment.
Source of data:	Contrail evolution model.
Any comment:	-

Parameter ID	**DXNZ 4**
Data/Parameter:	A
Data unit:	m^2
Description:	Gaussian plume area
Source of data:	A function of wind shear and diffusivities
Any comment:	-

Parameter ID	**DXNZ 5**
Data/Parameter:	V_T
Data unit:	$m\ s^{-1}$
Description:	Ice particle terminal velocity.
Source of data:	Spichtinger & Gierens 2009
Any comment:	-

Parameter ID	**DXNZ 6**
Data/Parameter:	I
Data unit:	$kg\ kg^{-1}$
Description:	Ice mass mixing ratio.

Source of data:	Contrail formation and evolution model.
Any comment:	-

Parameter ID	DXNZ 7
Data/Parameter:	r_{eff}
Data unit:	m
Description:	Effective radius
Source of data:	Function of r_{vol} and the ice habit dependent ratio C.
Any comment:	-

Parameter ID	DXNZ 8
Data/Parameter:	EI_{soot}
Data unit:	$kg\ kg^{-1}$
Description:	Emission index of soot from aircraft.
Source of data:	Model described in Section 7.4.48
Any Comment:	-

Parameter ID	DXNZ 9
Data/Parameter:	N
Data unit:	m^{-1}
Description:	Ice particles per contrail length.
Source of data:	Contrail formation and evolution model.
Any comment:	-

14.2 | Data and parameters monitored

14.2.1 |Two forms of monitoring occur under the project boundary. The first is the monitoring of real-world parameters linked to the flight that took place, to compare to the proposed OFP. The second form of monitoring consists of post-flight calculations carried out to verify flown trajectories, establish additional fuel burn, and confirm aircraft mass. In addition, numerical weather prediction models should be confirmed with scientific validation activity. Additionally, hindcast numerical weather prediction models may be used to assess the accuracy of the atmospheric forecast used in calculating the flight's CO2e impact, if such models are shown to add significant accuracy (>10%) in predicting key weather parameters. All project data shall demonstrably and verifiably be stored in a distributed ledger-based system enabling robust and centralised data management for secure and immutable storage, archived on

a flight-by-flight basis to enable future review by verification and validation bodies (VVBs) to establish (e.g.) that original OFP were created in a standard manner and without utilising external contrail management intelligence to 'game' OFP optimisation to maximise baseline/additionality differences.

Parameter ID	DXNZ 10
Data/Parameter:	Flight path
Data unit:	-
Description:	Latitude & longitude at waypoints along the flight.
Source of data:	Pre-flight, planned flight path is calculated from OFP. Post-flight, flown flight path is calculated using tracking data (GPS or ADS-B data).
Monitoring frequency:	Variable (from every few seconds to lower frequency).
QA/QC procedures:	In the US, ADS-B is the 'preferred method of surveillance for air traffic control', enabling greater capacity and safety levels due to its 'real-time precision'.[33]In light of this, QA/QC procedures for ADS-B data are not deemed necessary, other than in one scenario – see below. There is noise in the ADS-B data, but this is addressed by smoothing airspeed time series. Aircraft stored GPS data can also be used, as GPS data is the source of ADS-B.[34] It may be more accurate to obtain GPS data directly from aircraft, rather than ADS-B signal – thus, if GPS is used no QA/QC procedures will be implemented., *Scenario requiring QA/QC* Where aircraft fly over regions not fitted with ADS-B sensors, or with sensors that are faulty, QA/QC procedures are required to compare the calculated CO_2e for missing trajectory portions to calculations based on GPS data for comparable trajectories, to compensate for gaps in the flight trajectory data. The critical size of gap is set to 20km. If feasible, no sampling should be done and any flights with gaps should be run with GPS data. If this is not feasible due to a large number of flights, the sample size should be calculated using a sample size calculator[35] with the following inputs: - Expected mean: this can be refined after each round of QA/QC procedures, starting with 1. Here the quantity

[33] https://www.faa.gov/air_traffic/technology/adsb/atc
[34] https://www.faa.gov/air_traffic/technology/equipadsb/capabilities/ins_outs
[35] e.g. see hyperlink for sample size calculator inside table entry 'Guidelines for sampling and surveys for CDM project activities and programmes of activities' - https://cdm.unfccc.int/Reference/Guidclarif/index.html. See tab 'SRS-Mean'.

considered is the ratio of the modelled contrail CO_2e when using GPS data, to the modelled contrail CO_2e when using the ADS-B data with gaps (which have been interpolated within *pycontrails*), e_{Traj}.

- Expected standard deviation: similarly, it can be refined after each round of procedures but shall begin with a conservative 0.5.
- Confidence level: 95%
- Desired relative precision: 10%
- Population size: flights which have had significant gaps in ADS-B tracking data.

A minimum sample size of 30 will be used if the calculated number is below this threshold.

There is 95% confidence that the sample mean is representative of the population within an error of the relative precision value.[36] This relative precision is computed using the calculator provided with the following inputs: mean and standard deviation of the sample, the sample size employed, and the confidence level.

If the relative precision is < 10%, the sample should be considered as representative of the population. In this instance:

- if the sample mean, $\overline{e_{CO_2e_{Traj}}}$, is within range $0.9 - 1.1$, no further action should be taken.
- Otherwise, any credits generated using flights which had significant ADS-B gaps (greater than 20km) should have the contrail emissions in the modified flight (Equation 72, PE_i) scaled accordingly (by $\overline{e_{CO_2e_{Traj}}}$).

If the relative precision is > 10%, the sample is not considered as representative of the population. In this instance:

- The sample size should be doubled with the aim of achieving better convergence. If still no convergence is found as the sample size is repeatedly being increased, no sampling should be undertaken and all flights with large enough gaps will require GPS data and CO_2e calculations to be re-run.

Any comment:	This process requires logging large gaps in ADS-B data

[36] https://cdm.unfccc.int/sunsetcms/storage/contents/stored-file-20210531160756223/Meth_Stan05.pdf

	during the project. Calculating the gaps between points can be done straightforwardly in Python using the haversine function within *pycontrails*.[37]

Parameter ID	DXNZ 11
Data/Parameter:	$\dot{m}_f$
Data unit:	$kg\ s^{-1}$
Description:	Aircraft fuel flow (consumption) as a function of time.
Source of data:	See Section 7.4.50 for a description of how fuel flow is modelled.
Monitoring frequency:	Pre-flight (airline-supplied data); post-flight
QA/QC procedures:	*Pre-flight* It is not possible to assess the accuracy of the fuel burn estimates made in the baseline OFP which are used to estimate the contrail forcing of the baseline flight. *Post-flight* If Quick Access Recorder (QAR) data is used for the post-flight fuel flow analysis, no QA/QC procedure is required. If instead a scaled Poll-Schumann model estimate is used, post-flight total fuel burn measurements should be obtained from the airline for QA/QC purposes on a sample of flights which undertook deviations for contrail management. *Sampling technique* The quantity to be calculated is the ratio of the actual fuel burn to the estimated fuel burn in the modified OFP, e_{M_f}: $$e_{M_f} = \frac{M_{f_{actual}}}{M_{f_{Mod\ OFP}}}$$ The sample size should be calculated using a sample size calculator[38] with the following inputs: - Expected mean: this can be refined after each round of QA/QC procedures, starting with 1.

[37] See pycontrails/pycontrails/physics/geo on the *pycontrails* (Shapiro *et al.*, 2023) github for its definition.
[38] see hyperlink for sample size calculator inside table entry `Guidelines for sampling and surveys for CDM project activities and programmes of activities' - https://cdm.unfccc.int/Reference/Guidclarif/index.html. See tab 'SRS-Mean'.

- Expected standard deviation: similarly, it can be refined after each round of procedures but shall begin with a conservative 0.5.
- Confidence level: 95%
- Desired relative precision: 10%
- Population size: the number of flights which have undertaken contrail management.

A minimum sample size of 30 will be used if the calculated number is below this threshold. The mean and standard deviation of the sample dataset should subsequently be calculated and inputted into the relative precision calculator.

Although the fuel burn fed into the radiative forcing calculations may be scaled by a reduced value of $M_{f_{Mod\ OFP}}$ as described in 7.5g (if there are gaps in the aircraft trajectory data at the start or end), the total estimates will still be used (since $M_{f_{actual}}$ would have to be scaled too if the reduced $M_{f_{Mod\ OFP}}$ was used).

There is 95% confidence that the sample mean is representative of the population within an error of the relative precision value.[39] This relative precision is computed using the calculator provided[40] with the following inputs: mean and standard deviation of the sample, the sample size employed, and the confidence level.

If the relative precision is < 10%, the sample should be considered as representative of the population. In this instance:

- if the sample mean, $\overline{e_{M_f}}$, is within range $0.9 - 1.1$, no further action should be taken.
- Otherwise, the credits should be recalculated using a scale factor reduction or increase of the fuel flow in the post-flight analysis.

If the relative precision is > 10%, the sample is not considered as representative of the population. In this instance:

- more sampling can be done and the precision re-calculated, or
- the fuel flow ratio scaling factor should be reduced from 1 by 3x the difference between the calculated relative precision and the threshold 10% – this is one of the

[39] https://cdm.unfccc.int/sunsetcms/storage/contents/stored-file-20210531160756223/Meth_Stan05.pdf
[40] see hyperlink for sample size calculator inside table entry 'Guidelines for sampling and surveys for CDM project activities and programmes of activities' - https://cdm.unfccc.int/Reference/Guidclarif/index.html

	options laid out in the 'Sampling and surveys for CDM project activities and programmes of activities' document.[41] Credits should be recalculated using this scale factor.
Any comment:	-

Parameter ID	**DXNZ 12**
Data/Parameter:	Aircraft mass
Data unit:	kg
Source of data:	*Pre-flight* *i) Take-off mass* Airlines may provide estimates of take-off mass pre-flight as part of a package of information delivered to enable project developers/project practitioners to investigate potential contrail savings by altering the routes. If an aircraft take-off mass is not supplied, it can be estimated with *pycontrails* – using the method described in Section 7.4.51 (in which case this variable would not be monitored). It would be varied along the flight path in line with the modelled fuel flow. *ii) Variation through flight* If an estimate of the variation of aircraft mass or fuel burn through the flight is given, this is used to set the variable. Otherwise, a Poll-Schumann fuel flow estimate is used. *Post-flight* Airlines send an altered flight plan after receipt of recommendations – this will be used to extract the take-off mass for post-flight analysis. As above, if this is not supplied the take-off mass could still be estimated (Section 7.4.51). Subsequent variation of aircraft mass through the flight will be estimated using fuel flow data either supplied by the airline, or estimated through the Poll-Schumann method or other means.
Monitoring frequency:	Each flight
QA/QC procedures:	For each flight, the project developer/project practitioner will ingest aircraft mass data from xml package/*pycontrails* calculations/post-flight altered mass data, to be lodged in a secure distributed ledger-based database for immutable and transparent storage.

[41] i.e. if the relative precision was calculated as 13%, the scaling factor should be set to 1- 3(0.03) = 0.91.

Any comment:	-

Parameter ID	DXNZ 13		
Data:	Weather data		
Parameter:			Unit:
	p	pressure	Pa
	T	Temperature	K
	q	Specific humidity	$kg\ kg^{-1}$
		Specific cloud ice water content, or cloud ice water mixing ratio	$kg\ kg^{-1}$
	U	East-west wind speed	$m\ s^{-1}$
	V	North-south wind speed	$m\ s^{-1}$
		Lagrangian tendency of air pressure	$Pa\ s^{-1}$
	OLR	Outgoing longwave radiation	$W\ m^{-2}$
	SDR	Solar direct radiation	$W\ m^{-2}$
	RSR	Reflected solar radiation	$W\ m^{-2}$
Source of data:	Numerical weather prediction models, which have real-world observations fed into the initialisation of the models.		
Monitoring frequency:	Pre-flight		
QA/QC procedures:	Scientific validation comparisons of model predictions with in-situ observations such as radiosondes (as carried out, e.g., in Thompson *et al*., 2024) to be conducted for each new weather model iteration or version. The sample of radiosonde data should capture inter-seasonal as well as regional variability since this may impact the performance of the weather model. The regions investigated can be sampled from the regions in which contrail management will be undertaken. Thompson *et al*. (2024) should be referred to as an example study. This process should be completed before new versions of the weather model are used for contrail management.		
Any comment:	Validation activity can also take place via hindcast weather modelling where this is shown to add significant (>10%) accuracy		

Parameter ID	DXNZ 14
Data/Parameter:	Fuel % SAF blend
Data unit:	%
Description:	The % of the aircraft's fuel which is sustainable aviation fuel (rather than standard jet fuel).
Source of data:	Airline
Monitoring frequency:	If airlines are able and willing to supply data on % SAF blend for every flight in an automated way, monitoring will be undertaken on a per-flight basis. If not, a running fleet average % SAF blend, updated by the airline on a six-monthly basis, shall be used.
QA/QC procedures:	If fleet averaged values are used, an update shall be received from the airline every 6 months. This will be updated to every 2 months from 2030, as SAF usage is expected to rise significantly around this time.[42]
Any comment:	-

14.3 | General requirements for data and information sources

14.3.1 |The project system requires a range of data sources, some of which are proprietary, while others are open source. These include meteorological datasets, aircraft location datasets, aircraft performance datasets, and metadata on aircraft types and specific aircraft such as airframe type and engine type and age.

14.3.2 |The IT system that delivers the project will need to be able to assimilate and securely store these datasets, in order to provide input to the various models which calculate the contrail climate impact of a given flight.

14.3.3 |The data volumes may be considerable so there needs to be an extensible software architecture and an application programming interface into the respective third-party digital data sources.

14.4 | Sampling requirements

14.4.1 |Guidelines on the sampling required for aircraft fuel burn, aircraft trajectory and weather model verification are provided in the respective sections above.

[42] See e.g. UK and EU SAF blend targets for 2030:

- https://www.gov.uk/government/news/aviation-fuel-plan-supports-growth-of-british-aviation-sector
- https://www.easa.europa.eu/eco/eaer/topics/sustainable-aviation-fuels/saf-policy-actions#38

15| MONITORING REQUIREMENTS FOR ACTIVITIES WITH REVERSAL RISKS

15.1.1 |Not applicable.

16| APPLICATION TO PROGRAMME OF ACTIVITIES

16.1.1 |The methodology may be applied for standalone activities or a programme of activities (PoAs). In the latter case, the technology provider(s) may act as Coordinating and Managing Entity (CME). For inclusion of a Voluntary Project Activity (VPA) to the PoA, the inclusion criteria shall be designed following the methodology requirements and other applicable Gold Standard requirements.

17| RENEWAL OF CREDITING PERIOD

17.1.1 |This methodology is based on the best available current scientific literature. However, this is a currently active research field, so as the science advances, small changes will be made to models within the methodology to keep them up to date with the state-of-the-art.

ANNEX 1: INPUTS TO ENGINE NVPM EMISSION ESTIMATION

Engine Parameter	Variable name in input in *pycontrails*	Units
Engine unique identification number	UID	-
Engine pressure ratio (pressure of the exit of the compressor to the inlet)	Pressure ratio	-
Fuel flow rate, 7%	Fuel Flow Idle	$kg\ s^{-1}$
Fuel flow rate, 30%	Fuel Flow App	$kg\ s^{-1}$
Fuel flow rate, 85%	Fuel Flow C/O	$kg\ s^{-1}$
Fuel flow rate at take-off (used to estimate thrust setting)	Fuel Flow T/O	$kg\ s^{-1}$
nvPM Emission index at take-off (100% fuel flow)	nvPM EInum T/O	kg^{-1}
nvPM Emission index at 85% fuel flow	nvPM EInum C/O	kg^{-1}
nvPM Emission index at 30% fuel flow	nvPM EInum App	kg^{-1}
nvPM Emission index at 7% fuel flow	nvPM EInum Idle	kg^{-1}

ANNEX 2: INPUTS TO AIRCRAFT MODELLING

Aircraft parameter	Variable name in *pycontrails*	Unit
Year of first flight: this is used to estimate the turbine entry temperature at take-off using a function from Cumpsty & Heyes, 2015. In turn this is used to estimate the turbine entry temperature at max continuous climb, which is used in a calculation for the maximum allowable thrust coefficient.	Year_of_first_flight	-
Number of engines	n_engine	-
Winglets: yes/no	winglets	-
Reference wing area	Sref_m2	*m2*

$\cos(\Lambda_w)$: cosine of the wing sweep	cos_sweep	°
Wing Aspect ratio	AR	-
ψ_0: zero lift drag coefficients, defined as Cdo=CF× ψ0	psi_0	-
δ_2: induced drag wing-fuselage interference factor	delta_2	-
x_{ref}: condition related to the terminating shock wave in transonic flight moving downstream past a certain point on the airfoil.	Xo	-
wing_constant, j_1, j_2: wave drag parameters	Wing_constant, j_2, j_1	-
Fuel mass flow rate at engine idle and sea level static conditions: used to set fuel flow in operational limits if the calculated value is below this.	mf_idle_SLS_kg_s	$kg\ s^{-1}$
Fuel mass flow rate at take-off and sea level static conditions: used to set fuel flow in operational limits if the calculated value is above this.	mf_max_T_O_SLS_kg_s	$kg\ s^{-1}$
Optimum Mach number for minimum fuel flow	M_des	-
Optimum thrust coefficient (non-dimensional thrust) for minimum fuel flow	CT_des	-
η_1, η_2: coefficients describing optimum engine performance for a given Mach number	eta_1, eta_2	-
Weight variant: this is defined by the three aircraft masses below (Airbus, 2021).	WV	-
Maximum Take-off mass	MTOM_kg	*kg*
Maximum Landing mass	MLM_kg	*kg*
Aircraft maximum zero fuel weight	MZFM_kg	*kg*
Aircraft operating empty weight	OEM_i_kg	*kg*
Aircraft maximum payload	MPM_i_kg	*kg*

Maximum altitude (suggested in *pycontrails* that it could be used, in future, to approximate the minimum cruise flight level)	FL_max	*100×ft*
Maximum operational Mach number: this is used to clip the calculated flight Mach number if the aircraft is flying above 10,000 ft.	MMO	-
Total maximum thrust all engines can supply at sea level (not currently used in the code)	nominal_F00_ISA_kn	*kN*
Engine characteristic ratio of stagnation turbine-entry-temperature to stagnation freestream temperature (T_{04}/T_{01}) for maximum overall efficiency. This is used to estimate the maximum allowable thrust coefficient.	Tec	*K*
Associated Mach number with Tec. Like Tec this is also used to estimate the maximum allowable thrust coefficient.	Mec	-

ANNEX 3: CONSTANTS IN PYCONTRAILS

Parameter	Value	Units	Source (if supplied)
Vertical turbulent velocity perturbations, $\boldsymbol{\omega'_N}$	0.1	ms^{-1}	Schumann (2012)
Density of ice, $\boldsymbol{\rho_{ice}}$	*917*	kgm^{-3}	
Coefficients for formulae for turbulence and aggregation caused reduction in the number of ice particles, $\boldsymbol{E_A}$, $\boldsymbol{E_T}$	*1, 0.1*	-	The value for ET*ET* is 10x smaller than in Schumann's original paper. *pycontrails* explain their modification in the code, stating that the coefficient was calibrated using the observed lifetime and optical properties of contrails from the Contrail Library

			database, citing Schumann *et al.* (2017).
Specific heat capacity of combustion products, $c_{p_{comb}}$. This is used to estimate the turbine inlet temperature which is part of the nvPM particle estimation.	*1250*	$Jkg^{-1}K^{-1}$	
Solar constant	*1361*	Wm^{-2}	Paltridge (1976)
Weighting of different ice crystal geometries inside the contrail as the volume mean radius changes. The weighting chosen depends on the estimate for the volume mean radius of the ice crystals.	See [35]	-	Schumann *et al.* (2011)
Radiative forcing parameters for each ice crystal geometry	See [36]	-	Schumann *et al.* (2012)
Horizontal diffusivity coefficient, c_H	0.1	-	Schumann (2012)
A length scale used to estimate derivatives of temperature and velocity (for shear) in order to estimate the turbulent dissipation, which is used to estimate the downwash from the wake vortex, Δz_{eff}	*2000*	*m*	
Vertical diffusivity coefficient accounting for sedimentation, f_T	*0.5*	-	This value is a factor of 5 greater in *pycontrails* in comparison to Schumann 2012 following Schumann and Graf, 2013.
Vertical diffusivity coefficient accounting for turbulent mixing c_V, or $c_v\omega_N'^2$ (where c_v is a constant and ω_N' is a velocity measure of turbulent fluctuations) in Schumann 2012.	*0.01*	m^2s^{-2}	This is similarly enlarged in *pycontrails* following Schumann and Graf (2013).
Coefficient for the initial depth of the contrail (multiplying the maximum sinking due to the downwash), C_{D0}	*0.5*	-	Schumann (2012)

Wind shear enhancement coefficient, n	*0.5*	-	Schumann (2012) provides an equation, but *pycontrails* inserts it as a constant.
Max depth of the contrail: this is used to evaluate a maximum vertical diffusivity for the plume evolution calculation	*1500*	*m*	
Contrail resolution: if multiple flights are simulated at the same time, contrails separated by < dz_overlap_m are combined into 1	*500*	*m*	
Radiative forcing shortwave and long wave enhancement factors	*1, 1*	-	
Conditions for persistence of contrails - Duration < $20h$ - Optical depth: > 10^{-6}, < 10^{10} - Number of ice particles per volume of air: 10^3 < n < 10^{20} - Maximum segment length = 40km - $6000m$< Altitude < $13000m$ - Latitude not within $1°$ - of the poles		-	
Engine compressor efficiency	*0.9*	-	This is a typical value for modern turbofans
Conversion from r_{vol} to r_{eff} (C) for τ	0.9	-	Schumann (2012), citing Schumann *et al.* 2011

ANNEX 4: REFERENCES

- Abrahamson, J. P., Zelina, J., Andac, M. G., & Vander Wal, R. L. (2016). Predictive model development for aviation black carbon mass emissions from alternative and conventional fuels at ground and Cruise. Environmental Science & Technology, 50(21), 12048–12055. https://doi.org/10.1021/acs.est.6b03749
- Akhtar Martinez, C., & Jarrett, J. (2024). Comparing Two Contrail Models Under Certain and Uncertain Inputs. In AIAA SCITECH 2024 Forum (p. 1023).
- Bi, K., Xie, L., Zhang, H., Chen, X., Gu, X., & Tian, Q. (2022). Pangu-weather: A 3d high-resolution model for fast and accurate global weather forecast. arXiv preprint arXiv:2211.02556.
- Bickel, M., Ponater, M., Bock, L., Burkhardt, U., & Reineke, S. (2020). Estimating the effective radiative forcing of contrail cirrus. Journal of Climate, 33(5), 1991-2005.
- Bickel, M., Ponater, M., Burkhardt, U., Righi, M., Hendricks, J., & Jöckel, P. (2025). Contrail Cirrus Climate Impact: From Radiative Forcing to Surface Temperature Change. Journal of Climate, 38(8), 1895-1912.
- Bock, L., & Burkhardt, U. (2016). The temporal evolution of a long-lived contrail cirrus cluster: Simulations with a global climate model. Journal of Geophysical Research: Atmospheres, 121(7), 3548-3565.Bräuer, T., Voigt, C., Sauer, D., Kaufmann, S., Hahn, V., Scheibe, M., ... & Anderson, B. E. (2021). Airborne measurements of contrail ice properties—Dependence on temperature and humidity. Geophysical Research Letters, 48(8), e2020GL092166.
- Borella, A., Boucher, O., Shine, K. P., Stettler, M., Tanaka, K., Teoh, R., & Bellouin, N. (2024). The importance of an informed choice of CO 2-equivalence metrics for contrail avoidance. Atmospheric Chemistry and Physics, 24(16), 9401-9417.
- Chen, F., & Dudhia, J. (2001). Coupling an advanced land surface–hydrology model with the Penn State–NCAR MM5 modeling system. Part I: Model implementation and sensitivity. Monthly weather review, 129(4), 569-585.
- Chen, L., Zhong, X., Zhang, F., Cheng, Y., Xu, Y., Qi, Y., & Li, H. (2023). FuXi: A cascade machine learning forecasting system for 15-day global weather forecast. npj Climate and Atmospheric Science, 6(1), 190.
- Cumpsty, N., & Heyes, A. (2015). Jet Propulsion. Cambridge University Press.
- DuBois, D., & Paynter, G. C. (2006). " Fuel Flow Method2" for Estimating Aircraft Emissions. Sae Transactions, 1-14.
- Duda, D. P., Minnis, P., & Nguyen, L. (2001). Estimates of cloud radiative forcing in contrail clusters using GOES imagery. Journal of Geophysical Research: Atmospheres, 106(D5), 4927-4937.Dürbeck, T., & Gerz, T. (1996). Dispersion of aircraft exhausts in the free atmosphere. Journal of Geophysical Research: Atmospheres, 101(D20), 26007-26015.
- Fritz, T. M., Eastham, S. D., Speth, R. L., & Barrett, S. R. (2020). The role of plume-scale processes in long-term impacts of aircraft emissions. Atmospheric Chemistry and Physics, 20(9), 5697-5727.Galperin, B., Sukoriansky, S., & Anderson, P. S. (2007). On the critical Richardson number in stably stratified turbulence. Atmospheric Science Letters, 8(3), 65-69.
- Fuglestvedt, J.S., Shine, K.P., Berntsen, T., Cook, J., Lee, D.S., Stenke, A., Skeie, R.B., Velders, G.J.M. and Waitz, I.A. (2010). Transport impacts on atmosphere and climate: Metrics. Atmospheric Environment, 44(37), 4648-4677.
- Geraedts, S., Brand, E., Dean, T. R., Eastham, S., Elkin, C., Engberg, Z., ... & Goyal, N. (2024). A scalable system to measure contrail formation on a per-flight basis.

Environmental Research Communications, 6(1), 015008.Gultepe, I., & Starr, D. O. C. (1995). Dynamical structure and turbulence in cirrus clouds: Aircraft observations during FIRE. Journal of Atmospheric Sciences, 52(23), 4159-4182.

- Hansen, J., Sato, M. K. I., Ruedy, R., Nazarenko, L., Lacis, A., Schmidt, G. A., ... & Zhang, S. (2005). Efficacy of climate forcings. Journal of geophysical research: atmospheres, 110(D18).
- Hodnebrog, Ø., Aamaas, B., Fuglestvedt, J. S., Marston, G., Myhre, G., Nielsen, C. J., ... & Wallington, T. J. (2020). Updated global warming potentials and radiative efficiencies of halocarbons and other weak atmospheric absorbers. Reviews of Geophysics, 58(3), e2019RG000691.
- Holzäpfel, F. (2003). Probabilistic two-phase wake vortex decay and transport model. Journal of Aircraft, 40(2), 323-331.
- Iacono, M. J., Mlawer, E. J., Clough, S. A., & Morcrette, J. J. (2000). Impact of an improved longwave radiation model, RRTM, on the energy budget and thermodynamic properties of the NCAR community climate model, CCM3. Journal of Geophysical Research: Atmospheres, 105(D11), 14873-14890.
- ICAO (2018). ICAO Carbon Emissions Calculator Methodology version 11, June 2018. https://www.icao.int/environmental-protection/CarbonOffset/Documents/Methodology%20ICAO%20Carbon%20Calculator_v11-2018.pdf. (Accessed 17 April 2024).
- Immler, F., Treffeisen, R., Engelbart, D., Krüger, K., & Schrems, O. (2008). Cirrus, contrails, and ice supersaturated regions in high pressure systems at northern mid latitudes. Atmospheric Chemistry and Physics, 8(6), 1689-1699.
- Jeßberger, P., Voigt, C., Schumann, U., Sölch, I., Schlager, H., Kaufmann, S., ... & Gayet, J. F. (2013). Aircraft type influence on contrail properties. Atmospheric Chemistry and Physics, 13(23), 11965-11984.
- Jimenez, P. A., Hacker, J. P., Dudhia, J., Haupt, S. E., Ruiz-Arias, J. A., Gueymard, C. A., ... & Deng, A. (2016). WRF-Solar: Description and clear-sky assessment of an augmented NWP model for solar power prediction. Bulletin of the American Meteorological Society, 97(7), 1249-1264.
- Joos, F., Roth, R., Fuglestvedt, J. S., Peters, G. P., Enting, I. G., Von Bloh, W., ... & Weaver, A. J. (2013). Carbon dioxide and climate impulse response functions for the computation of greenhouse gas metrics: a multi-model analysis. Atmospheric Chemistry and Physics, 13(5), 2793-2825.
- Kaiser, M., Rosenow, J., Fricke, H., & Schultz, M. (2012, May). Tradeoff between optimum altitude and contrail layer to ensure maximum ecological en-route performance using the enhanced trajectory prediction model (ETPM). In ATACCS (pp. 127-134).
- Khan, A. H., Tait, K., Derwent, R. G., Roome, S., Bacak, A., Bullock, S., ... & Shallcross, D. E. (2023). Off-setting climate change through formation flying of aircraft, a feasibility study reliant on high fidelity gas-phase chemical kinetic data. International Journal of Chemical Kinetics, 55(7), 402-412.Koudis, G.S., Hu, S.J., North, R.J., Majumdar, A. and Stettler, M.E., (2017). The impact of aircraft takeoff thrust setting on NOX emissions. Journal of Air Transport Management, 65, pp.191-197.
- Kärcher, B., Burkhardt, U., Bier, A., Bock, L., & Ford, I. J. (2015). The microphysical pathway to contrail formation. Journal of Geophysical Research: Atmospheres, 120(15), 7893-7927Meijer, V. R., Eastham, S. D., Waitz, I. A., & Barrett, S. R. (2024). Contrail altitude estimation using GOES-16 ABI data and deep learning. Atmospheric Measurement Techniques, 17(20), 6145-6162.
- Le Clercq, P., Voigt, C., Sauer, D., Rauch, B., Bauder, U., Schripp, T., ... & Aigner, M. (2022). Emission and Climate Impact of Alternative Fuels. The ECLIF1 and ECLIF2 Campaigns. In 9th European Conference for Aeronautics and Space Sciences (EUCASS).

- Myhre, G., Shindell, D., Bréon, F. M., Collins, W., Fuglestvedt, J., Huang, J., ... & Zhang, H. (2014). Anthropogenic and natural radiative forcing. Climate Change 2013-The Physical Science Basis, 659-740.
- Märkl, R. S., Voigt, C., Sauer, D., Dischl, R. K., Kaufmann, S., Harlaß, T., ... & Le Clercq, P. (2024). Powering aircraft with 100% sustainable aviation fuel reduces ice crystals in contrails. Atmospheric Chemistry and Physics, 24(6), 3813-3837.
- Ng, J. Y. H., McCloskey, K., Cui, J., Meijer, V. R., Brand, E., Sarna, A., ... & Geraedts, S. (2023). Contrail Detection on GOES-16 ABI With the OpenContrails Dataset. IEEE Transactions on Geoscience and Remote Sensing.Olson, J. B., Smirnova, T., Kenyon, J. S., Turner, D. D., Brown, J. M., Zheng, W., & Green, B. W. (2021). A description of the MYNN surface-layer scheme.
- Paltridge, G. W., & R., P. C. M. (1976). Radiative processes in meteorology and climatology. Elsevier.
- Platt, J. C., Shapiro, M. L., Engberg, Z., McCloskey, K., Geraedts, S., Sankar, T., ... & Van Arsdale, C. (2024). The effect of uncertainty in humidity and model parameters on the prediction of contrail energy forcing. Environmental Research Communications, 6(9), 095015.
- Poll, I (2023, April). Advances in the modelling of aircraft cruise fuel burn and a new model for use in fleet environmental impact studies [Workshop presentation]. pycontrails workshop, Imperial College, London, UK
- Poll, D. I. A., & Schumann, U. (2021a). An estimation method for the fuel burn and other performance characteristics of civil transport aircraft in the cruise. Part 1 fundamental quantities and governing relations for a general atmosphere. The Aeronautical Journal, 125(1284), 257-295.
- Poll, D. I. A., & Schumann, U. (2021b). An estimation method for the fuel burn and other performance characteristics of civil transport aircraft during cruise: part 2, determining the aircraft's characteristic parameters. The Aeronautical Journal, 125(1284), 296-340.
- Ponater, M., Marquart, S., Sausen, R., & Schumann, U. (2005). On contrail climate sensitivity. Geophysical Research Letters, 32(10).
- Powers, J. G., Klemp, J. B., Skamarock, W. C., Davis, C. A., Dudhia, J., Gill, D. O., ... & Duda, M. G. (2017). The weather research and forecasting model: Overview, system efforts, and future directions. Bulletin of the American Meteorological Society, 98(8), 1717-1737
- Rap, A., Forster, P. M., Haywood, J. M., Jones, A., & Boucher, O. (2010). Estimating the climate impact of linear contrails using the UK Met Office climate model. Geophysical research letters, 37(20).
- Sausen, R., & Schumann, U. (2000). Estimates of the climate response to aircraft CO 2 and NO x emissions scenarios. Climatic Change, 44, 27-58.
- Schumann, U. (1996). On conditions for contrail formation from aircraft exhausts. Meteorologische Zeitschrift, 5, 4-23.
- Schumann, U., Konopka, P., Baumann, R., Busen, R., Gerz, T., Schlager, H., ... & Volkert, H. (1995). Estimate of diffusion parameters of aircraft exhaust plumes near the tropopause from nitric oxide and turbulence measurements. Journal of Geophysical Research: Atmospheres, 100(D7), 14147-14162.
- Schumann, U., Schlager, H., Arnold, F., Baumann, R., Haschberger, P., & Klemm, O. (1998). Dilution of aircraft exhaust plumes at cruise altitudes. Atmospheric Environment, 32(18), 3097-3103.
- Schumann, U., Mayer, B., Hamann, U., & Kasper, G. (2010a). Radiative heating in contrail cirrus. Geophysical Research Abstracts, 1-2. https://doi.org/https://elib.dlr.de/67811/

- Schumann, U., Mayer, B., Hamann, U., & Kasper, G. (2010b, May 2-7). Radiative heating in contrail cirrus [Conference Presentation]. European Geophysical Union General Assembly 2010, Vienna, Austria. https://elib.dlr.de/67811/
- Schumann, U., Mayer, B., Gierens, K., Unterstrasser, S., Jessberger, P., Petzold, A., ... & Gayet, J. F. (2011). Effective radius of ice particles in cirrus and contrails. Journal of the Atmospheric Sciences, 68(2), 300-321.
- Schumann, U. (2012). A contrail cirrus prediction model. Geoscientific Model Development, 5(3), 543-580.
- Schumann, U., Mayer, B., Graf, K., & Mannstein, H. (2012). A parametric radiative forcing model for contrail cirrus. Journal of Applied Meteorology and Climatology, 51(7), 1391-1406.
- Schumann, U., & Graf, K. (2013). Aviation-induced cirrus and radiation changes at diurnal timescales. Journal of Geophysical Research: Atmospheres, 118(5), 2404–2421. https://doi.org/10.1002/jgrd.50184
- Schumann, U., Penner, J. E., Chen, Y., Zhou, C., & Graf, K. (2015). Dehydration effects from contrails in a coupled contrail–climate model. Atmospheric Chemistry and Physics, 15(19), 11179-11199.
- Schumann, U., Baumann, R., Baumgardner, D., Bedka, S. T., Duda, D. P., Freudenthaler, V., Gayet, J.-F., Heymsfield, A. J., Minnis, P., Quante, M., Raschke, E., Schlager, H., Vázquez-Navarro, M., Voigt, C., & Wang, Z. (2017). Properties of individual contrails: A compilation of observations and some comparisons. Atmospheric Chemistry and Physics, 17(1), 403–438. https://doi.org/10.5194/acp-17-403-2017
- Schumann, U., Poll, I., Teoh, R., Koelle, R., Spinielli, E., Molloy, J., ... & Voigt, C. (2021). Air traffic and contrail changes over Europe during COVID-19: a model study. Atmospheric Chemistry and Physics, 21(10), 7429-7450.
- Shapiro, M., Engberg, Z., Teoh, R., Stettler, M., & Dean, T. (2023). pycontrails: Python library for modeling aviation climate impacts (v0.48.1). Zenodo. https://doi.org/10.5281/zenodo.10066949
- Skamarock, W. C., Klemp, J. B., Dudhia, J., Gill, D. O., Liu, Z., Berner, J., ... & Huang, X. Y. (2019). A description of the advanced research WRF version 4. NCAR tech. note ncar/tn-556+ str, 145.
- Spichtinger, P., & Gierens, K. M. (2009). Modelling of cirrus clouds–Part 1a: Model description and validation. Atmospheric Chemistry and Physics, 9(2), 685-706.
- Stettler, M. E. J., Boies, A. M., Petzold, A., & Barrett, S. R. H. (2013). Global Civil Aviation Black Carbon Emissions. Environmental Science & Technology, 130823150610008. https://doi.org/10.1021/es401356v
- Switch weight variant. Airbus Aircraft. (2021, November 18). https://aircraft.airbus.com/en/switch-weight-variant
- Tait, K. N., Khan, M. A. H., Bullock, S., Lowenberg, M. H., & Shallcross, D. E. (2022). Aircraft emissions, their plume-scale effects, and the spatio-temporal sensitivity of the atmospheric response: a review. Aerospace, 9(7), 355.
- Teoh, R., Engberg, Z., Schumann, U., Voigt, C., Shapiro, M., Rohs, S., & Stettler, M. E. (2024). Global aviation contrail climate effects from 2019 to 2021. Atmospheric Chemistry and Physics, 24(10), 6071-6093.
- Teoh, R., Schumann, U., Voigt, C., Schripp, T., Shapiro, M., Engberg, Z., ... & Stettler, M. E. (2022). Targeted use of sustainable aviation fuel to maximize climate benefits. Environmental science & technology, 56(23), 17246-17255.
- Teoh, R., Schumann, U., Majumdar, A., & Stettler, M. E. (2020). Mitigating the climate forcing of aircraft contrails by small-scale diversions and technology adoption. Environmental Science & Technology, 54(5), 2941-2950.
- Teoh, R., Stettler, M. E. J., Majumdar, A., Schumann, U., Graves, B., & Boies, A. M. (2019). A methodology to relate black carbon particle number and mass emissions.

Journal of Aerosol Science, 132, 44–59. https://doi.org/10.1016/j.jaerosci.2019.03.006

- Teoh,R., & Stettler, M (2023, April). Flight trajectories, aircraft performance and emissions [Workshop presentation]. pycontrails workshop, Imperial College, London, UK
- Thompson, G., Scholzen, C., O'Donoghue, S., Haughton, M., Jones, R. L., Durant, A., & Farrington, C. (2024). On the fidelity of high-resolution numerical weather forecasts of contrail-favorable conditions. Atmospheric Research, 311, 107663.
- Thompson, G., Politovich, M. K., & Rasmussen, R. M. (2017). A numerical weather model's ability to predict characteristics of aircraft icing environments. Weather and Forecasting, 32(1), 207-221.
- Thompson, G., & Eidhammer, T. (2014). A study of aerosol impacts on clouds and precipitation development in a large winter cyclone. Journal of the atmospheric sciences, 71(10), 3636-3658.
- UNFCCC (1997a). Kyoto Protocol to the United Nations Framework Convention on Climate Change. https://unfccc.int/resource/docs/convkp/kpeng.pdf. (Accessed 12th July, 2024).
- UNFCCC, FCCC/CP/1997/7/Add.1, Methodological issues related to the Kyoto Protocol, Secretary of the United Nations Framework Convention on Climate Change, Bonn, Germany, 1998
- Unterstrasser, S. (2020). The contrail mitigation potential of aircraft formation flight derived from high-resolution simulations. Aerospace, 7(12), 170.
- Vázquez-Navarro, M., Mannstein, H., & Kox, S. (2015). Contrail life cycle and properties from 1 year of MSG/SEVIRI rapid-scan images. Atmospheric Chemistry and Physics, 15(15), 8739-8749.
- Voigt, C., Kleine, J., Sauer, D., Moore, R. H., Bräuer, T., Le Clercq, P., ... & Anderson, B. E. (2021). Cleaner burning aviation fuels can reduce contrail cloudiness. Communications Earth & Environment, 2(1), 114.
- Voigt, C., Schumann, U., Jurkat, T., Schäuble, D., Schlager, H., Petzold, A., ... & Dörnbrack, A. (2010). In-situ observations of young contrails–overview and selected results from the CONCERT campaign. Atmospheric Chemistry and Physics, 10(18), 9039-9056.
- WRF Community (2000) "Weather Research and Forecasting (WRF) Model." UCAR/NCAR. doi: 10.5065/D6MK6B4K.
- Yu, F. (1998). A Study of the Formation and Evolution of Aerosols and Contrails in Aircraft Wakes: Development, Validation and Application of an Advanced Particle Microphysics (APM) Model. Doctoral Dissertation, UCLA.
- Yu, F.; Anderson, B.; Pierce, J.; Wong, A.; Nair, A.; Luo, G.; Herb, J. On nucleation pathways and particle size distribution evolutions in stratospheric aircraft exhaust plumes with H2SO4 enhancement. Environ. Sci. Technol. 2024, 58, 6934, DOI: 10.1021/acs.est.3c08408.

DOCUMENT INFORMATION

VERSION	DATE	DESCRIPTION
1.0	08/07/2026	First version released

PUBLISHED BY GOLD STANDARD

Contact Details

The Gold Standard Foundation
International Environment House 2
Chemin de Balexert 7-9
1219 Châtelaine Geneva, Switzerland
Tel +41 22 788 70 80
Email help@goldstandard.org